NAVIGATIONAL FEASIBILITY OF FLYBY / IMPACT MISSIONS TO INTERSTELLAR OBJECTS

A Thesis

presented to

the Faculty of California Polytechnic State University

San Luis Obispo

In Partial Fulfillment

of the Requirements for the Degree

Master of Science in Aerospace Engineering

By

Declan M. Mages

December 2019

COMMITTEE MEMBERSHIP

TITLE: Navigational Feasibility of Flyby / Impact Missions to Interstellar Objects

AUTHOR: Declan M. Mages

DATE SUBMITTED: December 2019

COMMITTER CHAIR: Eric Mehiel, Ph.D.
Interim Associate Dean

COMMITTEE MEMBER: Kira Abercromby, Ph.D.
Associate Professor

COMMITTEE MEMBER: Joe Carpico, B.S.
Aerospace Lecturer

COMMITTEE MEMBER: Shyam Bhaskaran, Ph.D.
JPL Outer Planet Navigation Group Lead

ABSTRACT

Navigational Feasibility of Flyby / Impact Missions to Interstellar Objects

Declan M. Mages

In October 2017, the first interstellar object, designated 1I/2017 U1 and more commonly referred to as Oumuamua, was detected passing through our solar system by the Pan-STARRS telescope, followed recently by the detection of 2I/Borisov in August 2019. These detections came much sooner than thought possible, and have redefined our understanding of the population of interstellar objects. With the construction of the next generation of powerful observatories, future detections are estimated to occur as frequently as two per year, and while there is significant scientific understanding to be gained from observing these objects remotely, a spacecraft sent to intercept one might be the only way to collect up-close, detailed information on the composition of an extra solar object. The ideal mission scenario would be a combination flyby and impact as performed and proven feasible by the Deep Impact encounter with the comet Temple 1. A study has already been done showing that trajectories to interstellar objects are feasible with current chemical propulsion and a "launch on detection" paradigm, with an estimated 10 year wait time between favorable mission opportunities, assuming future detection capabilities.

However, while a trajectory to one of these objects might be feasible, accurately performing a flyby and impacting an object with a hyperbolic orbit presents unprecedented navigational challenges. Spacecraft-target relative velocities can range between 10 km/s to 110 km/s with high phase angles between 90° and 180°. The goal of this thesis is to determine the required navigation hardware – an optical navigation camera and attitude determination system – which could provide high mission success probability for many potential encounter scenarios. This work is performed via a simulation program developed at the Jet Propulsion Laboratory that generates simulated images of a target during the terminal guidance phase of a mission, and feeds them into the algorithms behind autonomous navigation software (AutoNav) used for the Deep Impact mission.

Observations are derived from the images and used to perform target-relative orbit determination and calculate correction maneuvers.

ACKNOWLEDGMENTS

I would like to thank my wonderful parents who made me who I am today, who always believed in me my entire life, and who bestowed this incredible passion in me. I would also like to thank Shyam Bhaskaran for giving me the idea to investigate this thesis topic and for openly providing the tools and code to do so. Also, to Ed Riedel for providing the image simulation code. Paul Vetter also sacrificed part of his Thanksgiving holiday to read and edit this thesis, for which I am very grateful. And finally, to my advisor Dr. Eric Mehiel and my committee for providing me this incredible education.

TABLE OF CONTENTS

Page

LIST OF TABLES

LIST OF FIGURES

Figure Page

Chapter 1

INTRODUCTION

1.1 **Problem Statement**

Every year robotic spacecraft explore new destinations in the solar system, performing meaningful science in increasingly remote and challenging locations. From New Horizons flying by the most distant object ever explored in the Kuiper Belt in 2019, to Osiris-Rex orbiting the smallest asteroid ever orbited in 2018, missions push the boundaries of what is possible. In 2017 a new class of object was discovered, interstellar objects (ISOs), presenting a new challenge for exploration. These objects come as orphans from other solar systems elsewhere in the galaxy, and pass through our solar system at extremely high speeds on hyperbolic trajectories.

These ISOs provide a window into the composition of other solar systems, their surfaces would give information on effects of weathering in interstellar space, with recent studies suggesting these objects could be vehicles in which life is transported between planetary systems. The potential science returns from exploring one is immense. Project Lyra investigated rendezvous with an ISO and showed would require a heavy lift launch vehicle to launch a dozen kilogram spacecraft to then perform a Jupiter flyby and solar Oberth maneuver with solid rocket boosters and Parker Solar Probe heatshield technology just to catch up with a target [11]. Matching velocity would then require electric and magnetic sails. Ultimately, matching the hyperbolic orbits of ISOs is extremely challenging and potentially infeasible with current technology. An alternative investigated by this thesis is to intercept ISOs while they are within our solar system with a flyby spacecraft combined with an impactor spacecraft that strikes the ISO's surface releasing a plume of ejecta that the flyby spacecraft then images for subsurface compositional information. However, as these objects are on hyperbolic trajectories, they can appear with minimal warning thus requiring rapid response times to launch. The minimal warning time combined with their extremely high velocities, presents

unique challenges for sending a spacecraft to an ISO and accurately navigating an encounter in which meaningful science is performed.

1.2 **Proposed Solution**

Autonomous optical navigation is a powerful tool that has enabled several small body encounters over the past two decades. During the final two hours of a spacecraft's approach to a small body, the spacecraft autonomously images the target and performs relative orbit determination to continuously improve the spacecraft's knowledge of its relative state to the target. Without this autonomy, the spacecraft would have to attempt to image the target using the knowledge accuracy from the last ground update, which would typically be around 24 hours before encounter, which when dealing with the high orbital speeds of ISOs can be several million kilometers away. The accuracy at this distance would require the spacecraft to scan a large region of where the ISO could be and thus diminish the potential science returns and provide no chance of getting a spacecraft to impact. Autonomously refining the knowledge during the final hours would mean that more images taken during flyby would actually have the target in the field of view and would enable the accuracies required for impacting.

This thesis will first characterize the potential encounter environments that future ISOs might present. Relative velocity and phase angle are the two most important parameters (along with object size) that define how challenging an encounter is. With the realistic encounter environments constrained, this thesis then seeks to determine what equipment – primarily the camera and attitude determination system – will enable accurate autonomous optical navigation and broad mission success across the realistic encounter space. This is accomplished by fully simulating the critical final two hours of each encounter scenario. This is done by propagating equations of motion and generating images that are fed into the mathematical models of the autonomous navigation system to perform orbit determination and calculate correction maneuvers. Each encounter scenario is simulated multiple times and a Monte-Carlo analysis is performed to estimate success rates.

1.3 **Past Missions and Research**

Flybys have been a key class of space missions from the beginning of the space exploration era. They have been executed on every planet and on numerous small bodies. The list of asteroids includes 951 Gaspra, 243 Ida, 253 Mathilde, 433 Eros, 9969 Braille, 5535 Annefrank, 25143 Itokawa, 2867 Steins, 21 Lutetia, 4 Vesta, 4179 Toutatis, 1 Ceres, 101955 Bennu, and 486958 Arrokoth. Along with comets Giacobini-Zinner, Halley, Grigg-Skjellerup, Borelly, Wild 2, Tempel 1, Hartley 2, and Churyumov-Gerasimenko. The most relevant to this ISO mission concept are small body encounters where the spacecraft used autonomous optical navigation. This capability was developed at the Jet Propulsion Laboratory and was first demonstrated on the mission Deep Space 1 [21], and has since enabled the flybys of comets Borrelly, Wild 2, Tempel 1, Hartley 2, and asteroid Annefrank. These establish the fundamental method in which an encounter with an ISO would be navigated.

The NASA mission Deep Impact and its encounter with comet Tempel-1 illustrates the only time that a combination flyby and impact has been implemented and therefore forms the foundation from which this thesis builds off. The flyby spacecraft released a small 350 kg impactor spacecraft 24 hours prior to encounter. This impactor spacecraft then autonomously guided itself to collide with Temple-1 at 10.3 km/s while the flyby spacecraft also operating autonomously imaged the target and resulting ejecta [15]. The encounter sequence had the flyby and impactor spacecraft imaging the comet every 15 seconds, compiling 4 images before performing an orbit determination update and executing targeting maneuvers at 100 min, 35 min, and 7.5 min from impact. This encounter sequence design [14] gives the baseline sequence design from which the terminal phase of an interstellar visitor flyby/impact is simulated in this thesis.

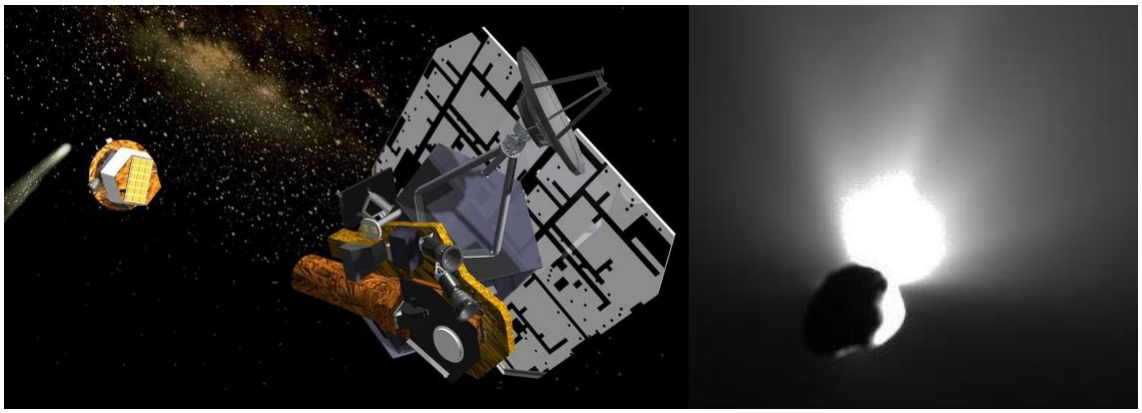

Figure 1.1: Artist's rendition of Deep Impact spacecraft and encounter image taken by the flyby spacecraft of the impactor colliding with Tempel-1.

The most relevant prior research for this thesis is by Shyam Bhaskaran and Brian Kennedy of NASA's Jet Propulsion Laboratory [1]. They expanded on the success of Deep Impact's autonomous navigation and investigated the general navigational feasibility of impacting and deflecting a wide range of asteroids with varying sizes, relative velocities, and approach angles via simulation and Monte Carlo analysis. The scenarios investigated and the resulting success rates given different attitude determination methods are outlined in Table 1.1.

Table 1.1: Probability of asteroid impact.

Case		Stellar Reference		SSIRU	
V_∞ (km/s)	Phase Angle (deg)	100 m	300 m	100 m	300 m
7.5	30	98.8%	100.0%	85.5%	100.0%
7.5	80	96.5%	100.0%	73.8%	99.2%
12.5	140	56.6%	99.4%	53.8%	90.6%
20	5	100.0%	100.0%	75.4%	99.6%

An important conclusion from their analysis showed that attitude error is the most critical parameter in determining mission success. When entering the terminal guidance phase of a flyby/impact mission, the target often becomes significantly brighter than the background star which prevents imaging of both simultaneously. The stars are typically used to determine the

attitude of each image, and without them the spacecraft is required to instead rely on its IMU for attitude determination. The errors associated with using an IMU are significantly greater than when using stellar reference and are discussed in greater detail in 3.3. This effect of this IMU error was highlighted by the results of their simulations which showed that without the most accurate inertial measurement unit available, the Scalable SIRU (SSIRU) [31], the likelihood of impacting smaller asteroids drops significantly as shown in Figure 1.2.

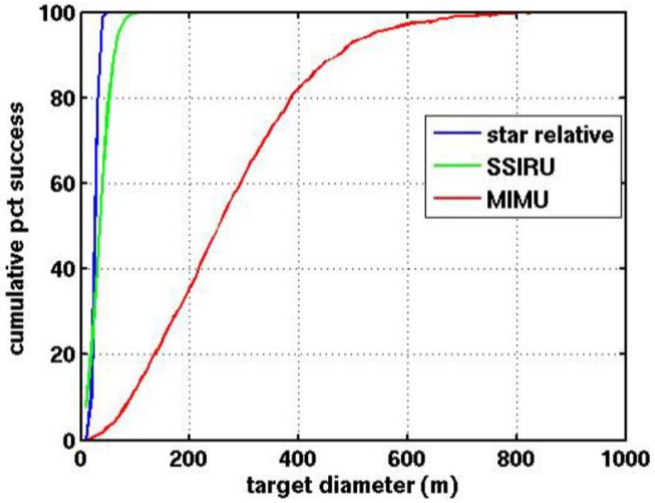

Figure 1.2: Cumulative probability as a function of target diameter for three attitude modes [1].

The results of this analysis showed that the most significant parameter in determining impact success was the attitude error and phase angle, while higher velocities up to 20 km/s did not seem to significantly affect the success rate. Unfortunately, as analysis later shows in section 4.2, 20 km/s is on the low end of potential relative velocities ISOs may present.

The highest relative velocity flyby to date was with Halley's Comet at 68 km/s. Multiple spacecraft were sent to Halley and navigated using only radiometric tracking and without the use of optical navigation. With consecutive distant flybys (~8000 km) from multiple spacecraft, Halley's ephemeris was refined [10] and made accurate enough for the closest flyby by the Giotto spacecraft at 600 km. This technique proved successful and resulted in the first-ever images of a comet nucleus, but it only provided a relative state knowledge accuracy of roughly 40 km. This

was sufficient as Halley is a large body around 15 km x 9 km and the highest resolution image was taken 5 minutes before closest approach at a distance of 20,000 km. However, as ISOs are potentially much smaller bodies, the resolution achieved with this level of accuracy would be unacceptable. The accuracies required for a flyby and impact mission of an ISO in the hundreds of meters size is an order of magnitude greater than achieved in the Halley encounters, and so ultimately little can be said about these missions and their feasibility based on the Halley flybys.

Another relevant mission is the flyby of asteroid Annefrank. Executed primarily as systems test for the Stardust spacecraft before its encounter with Wild 2, this flyby was unique for its approach phase angle of 130°. This is the highest for a flyby ever, yet still is only in the middle of the range that ISOs might present. Annefrank's high phase angle combined with a much dimmer surface than expected meant the optical navigators were unable to detect it during approach and before the initialization of the autonomous phase [2]. Even under these circumstances the spacecraft was able to identify Annefrank when it got brighter and track it during encounter. This is an important reference mission because the ISO high phase angles will likely result in very dim targets that may not be detectable during approach, as I discuss in Section 4.3.

Chapter 2

A FLYBY & IMPACT MISSION

2.1 **Interstellar Objects**

The first step in understanding how to execute a mission is understanding the target, ISOs. Looking at our own solar system, it is theorized that the early belts of small bodies were heavily depleted by the gravitational perturbations of the giant plants [25]. These objects were ejected and sent to drift through the interstellar medium, a preserved sample of their home solar system. It was initially believed that with the construction of the Large Synoptic Survey Telescope (LSST), there was a possibility that these objects might be detected passing through our own solar system [16]. And then, significantly ahead of schedule, the first interstellar object (ISO), designated 1I/2017 U1 and more commonly referred to as Oumuamua, was detected passing through our solar system by the Pan-STARRS telescope in October 2017 with a hyperbolic escape velocity of 26.3 km/s [Figure 1.1]. Very quickly Oumuamua was found to have interesting properties. Its brightness varied by a magnitude of 10 over its 7-hour rotational period – a larger variation than anything else observed in our solar system -- suggesting a very elongated shape. It was initially assumed to be a comet, but when no coma was detected, it was classified as an asteroid. However, while observing Oumuamua's outbound trajectory, it had clearly been affected by some acceleration inconsistent with solar gravity. There are many theories that attempt to explain this, with the most prevalent being that Oumuamua actually was comet-like and experienced small amounts of outgassing during its approach with the sun [25]. Much is unclear about Oumuamua, and now that it is forever beyond observational range, much will remain unclear. Because this detection was much sooner than thought possible, it redefined our understanding of the population of interstellar objects. Multiple studies now have estimated densities of these objects to be around ~$0.1/AU^{-3}$, which implies that on average, at any given time at least one interstellar object is passing within a 1.35 AU radius

sphere centered at the sun. Estimates then predicted that with the construction of the LSST, future detections might be as regular as two per year, with higher estimates of ten per year [7].

Astronomers were shocked again by the discovery of 2I/Borisov [10]. First identified in August of 2019 as an unknown object on a peculiar orbit, it was confirmed within weeks to be of interstellar origins with a hyperbolic escape velocity of 32.2 km/s [Figure 2.1]. 2I/Borisov had a clear cometary coma, quite different from Oumuamua. Its discovery was also different from Oumuamua's, as it was found while still headed into the solar system, with its closest approach to the Sun still to occur on December 8th 2019. This has provided ample opportunity for observation and characterization with the latest data suggesting it has similar properties to our solar system's long period comets and Oort cloud comets. As 2I/Borisov's body is hidden by its coma only rough estimates of its size can be made. Initial estimates suggested a diameter range of 2 to 16 km, with more recent estimates claiming a range between 1.4 and 6.6 km. Given this small size, astronomers will look to see if it disintegrates as it nears its closest approach distance of 1.9 AU. With this discovery the number of known ISOs has doubled, but since both objects have entirely different properties, their mystery has only deepened.

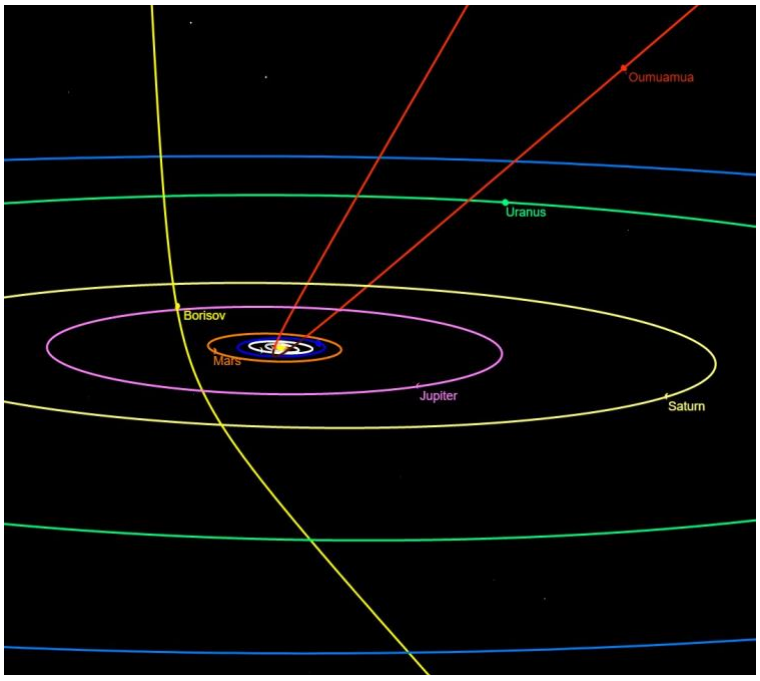

Figure 2.1: Oumuamua's and 2I/Borisov's orbits through our solar system.

2.1.1 Intercept Trajectories

Before a mission to an ISO can be considered from a navigational standpoint, we should understand whether trajectories to intercept future ISOs will even be possible with current launch vehicle capabilities. With funding from NASA, Darryl Seligman and Gregory Laughlin investigated this by modeling the estimated population of interstellar objects in our galaxy, the possible paths they might take through our solar system, the detection capabilities of the LSST to estimate detection rates [24]. From there they estimated the rate at which interstellar objects would enter our solar system on orbits that present favorable intercept trajectory opportunities. They concluded that with the LSST, and with a "launch on detection" paradigm (meaning that a spacecraft is already built before initial detection), mission opportunities would present themselves roughly every 10 years. They estimated a median total ΔV required for these opportunities to be 12 km/s. While this is large, it is feasible with heavy launch vehicles such as the Delta IV Heavy and Falcon Heavy, and a spacecraft with several km/s of onboard ΔV capability. This study was conducted before the additional detection of 2I/Borisov which has likely significantly changed the best estimates of ISO population densities.

Using Oumuamua's orbit as an example, it presented extremely favorable intercept trajectory opportunities (had it been detected early enough), with potential impacting on October 26th 2017 requiring ΔV from Earth of only 4 km/s. Using JPL's online mission design tool [32], we see that there were multiple months during which a multi-thousand-kilogram spacecraft could have been launched to intercept Oumuamua [Figure 2.2]. For 2I/Borisov, it needed to be detected before July 2018 to enable the launch of a 2000 kg spacecraft on a heavy launch vehicle for an encounter in October 2019. The orbits for both these intercept trajectories are presented in Figure 2.3.

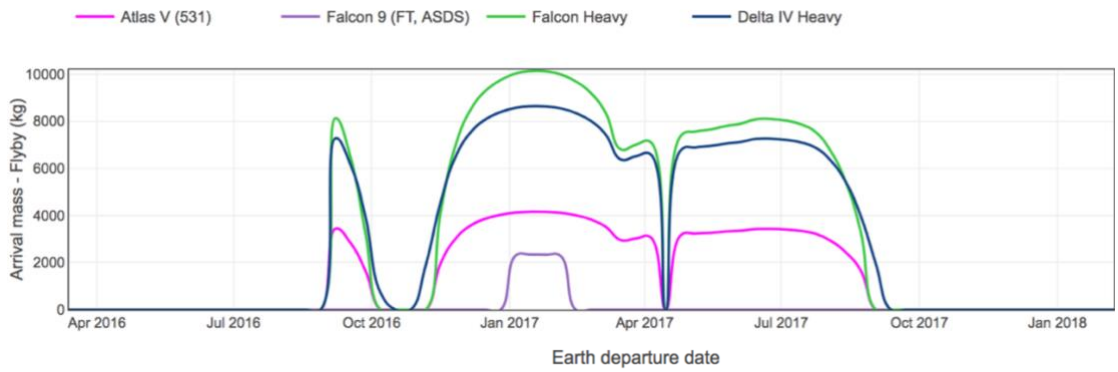

Figure 2.2: Spacecraft mass vs departure date from intercept trajectories to Oumuamua.

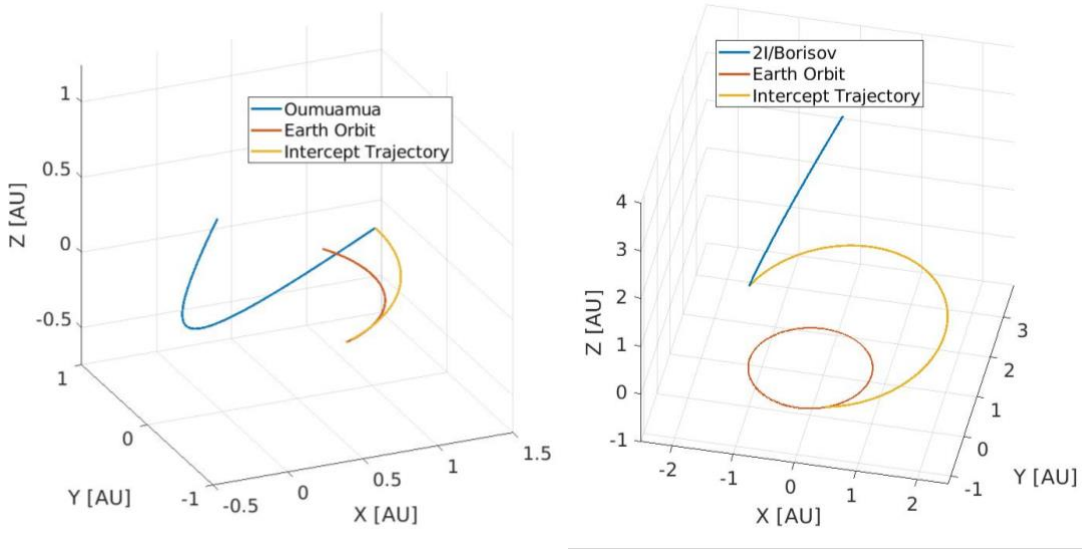

Figure 2.3: Orbits of Oumuamua and 2I/Borisov and their corresponding intercept trajectories.

2.2 Navigating a Flyby/Impact

Having shown that intercept trajectories are possible with heavy launch vehicles and/or onboard propellant, navigation to a hyperbolic-orbit object is the next part of this problem. Navigation is particularly difficult since the "launch on detection" paradigm requires a spacecraft to be designed without knowledge of its eventual encounter scenario. Fundamentally, executing a flyby and impact mission to a target demands two knowledge requirements be satisfied. First, the flyby spacecraft needs to know its own relative state to the target well enough to flyby at a desired location while pointing the instruments on target to achieve its science goals, the most demanding of which is

often the high- resolution close approach imaging. Second, the impactor spacecraft needs to know its relative state to the target well enough to impact an illuminated portion of its surface. Initially the relative state between target and spacecraft is known from independently having solutions for the target's orbit and the spacecraft's trajectory, and differencing the two. The target's orbit solution is primarily generated from ground-based or space-based optical observations, while the spacecraft's trajectory is known via radio tracking data such as Doppler and Delta-Differential One-Way Ranging (ΔDOR). The state error for most asteroids is on the order of tens of kilometers in position and several cm/s in velocity, while spacecraft state knowledge is also often in the low tens of kilometers and cm/s range. Together these errors result in a target relative error that would make it impossible to get detailed close approach images or get close to impacting potential even multi kilometer sized bodies. These errors must be reduced [or corrected] to achieve mission science goals.

2.2.1 Optical Navigation

An effective way to reduce this error is through optical navigation. Optical navigation is the process of imaging the target with an imager that is onboard the spacecraft itself, shown schematically in Figure 2.4. Images are sent back to the ground and processed by the navigation team who locate the target in the image and use the background stars to determine the pointing of the image. Together that forms an observation of the target, which is used to perform target-relative orbit determination. The nature of this data being target-relative, means it directly observes the key knowledge of interest, the relative state to the target, thus mitigating the individual state errors of the target orbit and spacecraft trajectory. Also, as optical navigation data is angular it gets more accurate as the spacecraft gets closer, which leads to extremely powerful measurements during the final few hours of approach.

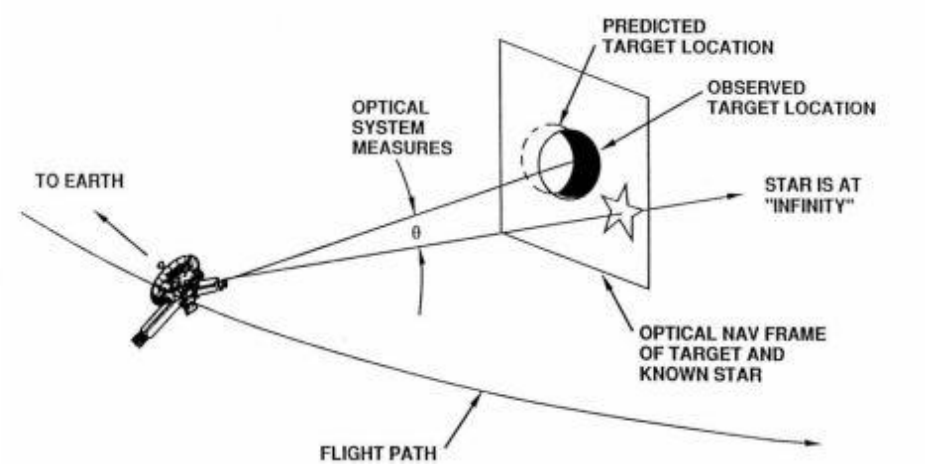

Figure 2.4: Optical navigation diagram from Matt Bergman [5].

2.2.2 Autonomous Optical Navigation

Only by operating autonomously can a spacecraft capitalize on these extremely powerful images taken during the final few hours of approach since the turnaround time of ground communication is prohibitive. Spacecraft have operated autonomously in this fashion many times before in previous missions, utilizing the software AutoNav, developed at the Jet Propulsion Laboratory. AutoNav was first demonstrated on the mission Deep Space 1, and has since enabled flybys of comets Borrelly, Wild 2, Tempel 1, Hartly 2, and asteroid Annefrank [20], [20]. Utilizing AutoNav for terminal phase observations is required to achieve enough knowledge accuracy for an impact mission, and due to the nature of ISO's extreme hyperbolic velocities and often poor illumination detailed later, the object might only be first detected by AutoNav during this period. This thesis will therefore focus on analyzing the terminal phase of possible ISO encounter scenarios to determine the feasibility of accurately performing a combination flyby and impact mission.

2.2.3 Determining Feasibility

AutoNav's ability to successful navigate an encounter is defined by a complex interaction of many spacecraft subsystems. A more detailed breakdown is given in AutoNav's Technology

Validation Report [21], while a simplified version of how the subsystems come together and interact is depicted in Figure 2.5.

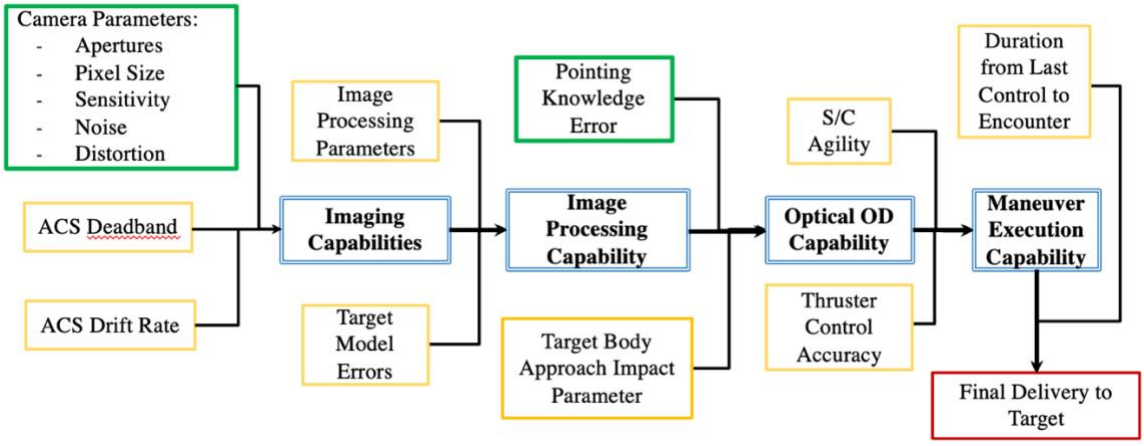

Figure 2.5: Breakdown of spacecraft subsystem interaction with AutoNav. Green identifies the most important parameters that are investigated in this thesis.

Breaking this figure down from left to right, the first parameters to consider are the quality and design of camera itself and the spacecraft's attitude control system (ACS) for stable pointing. Together these define the camera's ability to image. With the accuracy of the target model and the image processing included, the overall ability to derive and observation from an image is defined. The approach impact parameter describes the location of where the spacecraft will fly by the target. At greater distances the spacecraft can measure parallax and thus gain insight on the distance to the target. This effect combined with pointing knowledge errors defines the overall optical orbit determination (OD) capability. Then the spacecraft's agility and thruster accuracy define the ability to execute maneuvers, which together with the time of last control defines the final delivery to the target.

The most critical of these parameters that define a majority of the AutoNav system's ability to succeed are; 1 - the camera instrument and 2 - the attitude determination system (outlined Green in Figure 2.5). These systems are the most important because they define the accuracy of the optical observations. The camera's angular resolution directly translates to the angular accuracy of the observed target's center. That combined with the attitude knowledge at the time each image is

taken, defines the total angular accuracy of the observation. The ACS system is typically designed to stability requirements that are defined by the camera, while proper image processing parameters can maximize the accuracy of an observation the effect is an order of magnitude less than the camera and attitude system's errors. More capable cameras and attitude determination methods will produce more accurate observations which then produce a more accurate relative state estimation, which, if accurate enough and with the required propulsive agility, enables impact and the desired flyby images. By simulating the terminal phase of possible encounter scenarios while varying the capabilities of these systems, this thesis seeks to develop understanding of what is required for high impact and flyby imaging success rates across potential ISO mission scenarios.

Chapter 3

PROBLEM SETUP

3.1 **Overview**

The simulation program used for this analysis was taken directly from Jet Propulsion Laboratory spacecraft navigators Bhaskaran and Kennedy who initially used the program to investigate the challenges of navigating to and impacting small asteroids. Their software was taken and modified for the distinct encounter scenarios involved with ISOs and so much of this section repeats the concepts they outline. Reference [1] gives more detailed explanations of much of the mathematical models behind the simulation while a general overview is included here. The terminal guidance simulation begins with the truth target-relative state two hours from encounter, which is controlled as an input to define the relative velocity and encounter phase angle. Knowledge errors are applied to this state to approximate the error from the last orbit determination done with the ground in the loop. Next, simulated images are generated based on the state, the spacecraft's camera properties, and the input physical characteristics of the target. The simulated images are then processed to determine the center of brightness of the target, which along with the attitude knowledge associated with the image, defines an observation. Once several observations are taken, orbit determination is performed to update the estimate of the state. Then at predefined times, the required correction maneuver is calculated and 'executed' with errors and applied to the state. This process is repeated until the last maneuver is applied to the state and propagated to determine impact success. A breakdown of the inputs, mathematical models, and methods involved in this simulation is presented in the rest of this chapter.

3.2 **Camera**

The spacecraft's camera is the primary instrument that defines the angular accuracy of the observed center of the target in each image. A camera works by collecting light through a series of apertures and lenses that focus the light onto the camera's detector, often a charge-coupled device (CCD), which converts the amount of light collected on each pixel into photoelectrons which are then measured and recorded as an array of data numbers or DN values to define a picture. The goal with each picture is to derive the center of the target and the centers of cataloged stars also captured in the image. While the target is unresolved (smaller than a single pixel), its signal is still diffracted and slightly blurred from diffraction and imperfect optics, resulting in a shape called the camera's point spread function (PSF). Centerfinding techniques such as fitting to a light envelope function (e.g. Gaussian) can be applied to the PSF to locate the center of the target. These methods typically have accuracies on the order of a tenth of a pixel when the target source has a good signal to noise. When the target becomes resolved, other methods such as limb scanning or a brightness moment algorithm can be used to derive the center. The accuracies of these methods depend on several factors including how well the target is illuminated and how well its shape is known. Generally, the accuracy is inversely proportional to the size of the target in the image.

In using one of these centerfinding methods, the observed center is found in the pixel coordinate system of the image: sample and line (s, l). The sample and line location of the center needs to be converted into its physical location on the detector. This is accomplished via a simple 2x2 transformation matrix that describes the physical dimensions of a pixel, often in mm/pixel. With the physical location on the detector known, the next step is to derive what vector, as described in the coordinates of the camera, that location projects into. For an ideal camera, the location of the observed center translates directly into a vector based on the focal length as illustrated in Figure 3.1. However, cameras are never ideal and thus distort the projected image. The primary aberrations are radial distortion, and tip and tilt misalignment. These effects are carefully measured before

launch so that simple corrections can be applied to the observed center location to adjust it to its 'ideal' camera location. Next a simple conversion based on focal length gives a physical vector within the camera. This vector within the camera can then be converted to a vector within inertial space given knowledge of the camera's attitude at the time of the image.

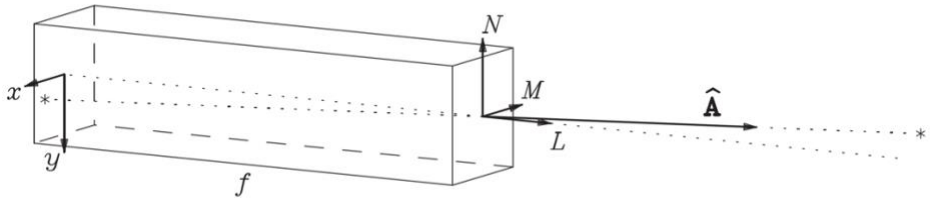

Figure 3.1: A pinhole camera showing a gnomonic projection for a star [19].

It is important to highlight the importance of the pixel size in deriving accurate observations as the origin of this vector observation is derived from centerfinding techniques that have accuracies proportional to the pixel. This means that smaller the angle subtended by a single pixel (the instantaneous field of view (IFOV)), the more accurate the center is in metric space. Also, the smaller the IFOV, the sooner the target becomes resolved and the particular illuminated portion of it can be targeted. The IFOV can be reduced by two ways, increasing the focal length of the camera or decreasing the physical pixel's size. The relationship is presented in equation 3.1, where f is the focal length and K describes the size of the pixel in pixels/mm.

$$\text{IFOV} = K / f \tag{3.1}$$

Developing and verifying new space rated CCD detectors with smaller pixels to the levels required for interplanetary spacecraft is a long and expensive process. Increasing focal length to decrease the IFOV, while straightforward in principle also increases camera size and cost. This is an extremely simplified description of camera design, but the basics of this tradeoff is the primary focus of this thesis, since with a high enough IFOV, observations can in principle become so accurate that any navigational challenge can be overcome. Thus, the question becomes: how accurate of a camera is needed to give high success rates for all realistic ISO encounter scenarios?

3.3 **Attitude Determination**

The attitude of the camera is described by three angles, right ascension, declination, and twist. The right ascension and declination together describe where the center of the camera is pointed (L in Figure 3.1), while twist describes the camera's rotation about that axis. These angles define rotation matrices that transform camera coordinates to the inertial frame. The most accurate method for determining the attitude of every image is through the stars in the image itself. This can be done as long as at least two (and ideally three or more) cataloged stars appear in the image along with the target. Again, highlighting the effect of a small IFOV, the pointing accuracy of this method depends on the centerfinding of the stars, which too is dependent on the size of the pixel. An issue arises when the target becomes so bright that shorter exposures are needed which fail to capture enough background stars. When exactly this happens depends a variety of factors which are discussed further in section 4.3. Regardless, one solution is to take alternating frames with different exposure times to capture the dimmer background stars, then the target and then the background stars again, referred to as flash-flash imaging in this thesis. Assuming the spacecraft has a constant drift rate and direction during this image sequence one can interpolate between the derived attitude of the star images to determine the attitude of the target image. The drawback to this method is a reduced number of actual target observations for orbit determination. Alternatively, and what has always been done in the past, one can rely on the spacecraft's own attitude determination system. This consists primarily of the IMU, which takes the attitude handed off at the beginning of terminal guidance and propagates it throughout the terminal phase to give an associated attitude with every image. Analysis has been done on use of star trackers to compliment the IMU during the terminal phase, and the conclusion drawn was that it is optimal to leave the star trackers off during the terminal guidance phase to avoid the sudden attitude error shifts that occur when stars move in and out of the tracker frame, called the "star tracker spatial error" problem [1]. The dominant errors

that are introduced into the solution are a result of the IMU's initial attitude bias and the angle random walk error that propagates over time.

3.4 **Orbit Determination**

Once a series of optical navigation observations of the target are made, orbit determination can be performed. The observations are combined and batch-filtered and fit via a least-squares method to improve the state estimate at a given epoch which is then propagated forward to the desired times. The full state vector (X) defined in equation 3.2 is comprised of the position and velocity components and the pixel bias (P) and line bias (L) measurements and their rates.

$$X = [\, x \quad y \quad z \quad \dot{x} \quad \dot{y} \quad \dot{z} \quad P \quad \dot{P} \quad L \quad \dot{L}\,] \tag{3.2}$$

The full AutoNav flight code utilizes a full dynamic model that integrates equations of motion that include accelerations from the Sun, planets, and solar radiation pressure. However, for this simulation the target relative motion is simplified and modeled as straight-line motion. Inaccuracies in the modeling of the gravitational forces and solar radiation pressure have little effect in the simulated two-hour terminal guidance period while the computational speed gained from this simplification is extremely significant. The orbit determination (OD) follows the standard mathematical process of least squares fitting. The partial derivatives of the pixel and line observations with respect to the parameters in the state vector are calculated. How to calculate the partials with respect to the position and velocity components is outlined in [19], while the partials with respect to the biases are simple derivatives. With the partials, the data weights, the observation residuals, and an initial guess, the least squares fit is calculated, and after several iterations, converges to a solution. More details of the simulation's OD process, such as the data weights, are outlined by Bhaskaran and Kennedy in [1].

3.5 **Maneuver Computation**

The navigational goal of a flyby / impact mission is to deliver the flyby spacecraft to a desired flyby location relative to the target and deliver the impactor into the target. These locations and the spacecraft's miss distance are represented in the B-plane coordinate which is classically utilized for flybys and gravity assists. As depicted in Figure 3.2, the B-plane is centered on the target and is perpendicular to the spacecraft's incoming asymptote with axis denoted *T* and *R*. *T* is normal to the incoming asymptote and typically lies parallel to the ecliptic or the J2000 equator. *R* is then defined by the cross product of the incoming asymptote and *T*. The last dimension along the asymptote is described by the linearized time of flight (*LTOF*), which is the spacecraft's position divided by the relative velocity. The figure depicts the use of the B-plane for a gravity assist around a planet, in which case the spacecraft's trajectory is significantly diverted from its original incoming asymptote. As we are dealing with small bodies with minimal gravitational fields, the approach and departing trajectories are effectively the same, and again the relative motion is modeled as a straight line.

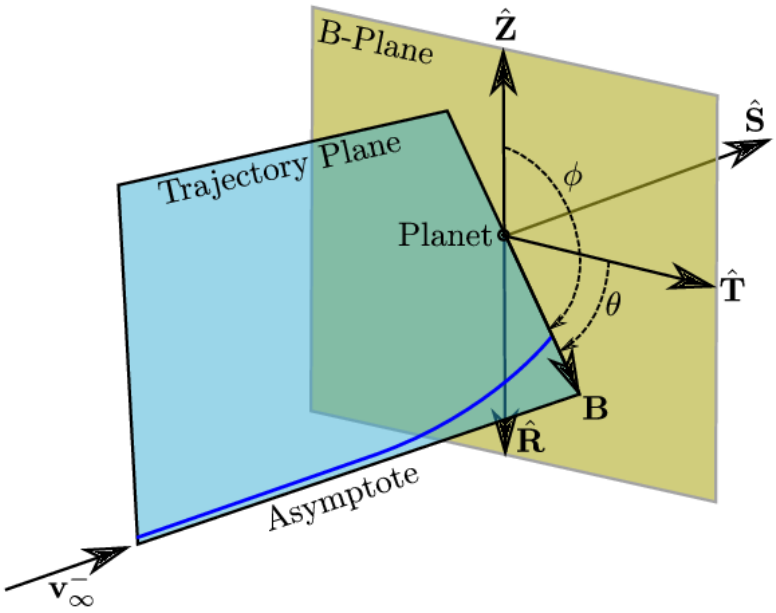

Figure 3.2: B-plane coordinate system.

The goal of a maneuver is to eliminate any offsets in the B-plane from the desired delivery. As the encounter is linearized the calculation to determine the required ΔV vector is straightforward. A targeted parameter Z is defined which contains the desired location in R and T, and the desired $LTOF$. For impacting these are all zero. For a flyby spacecraft it is assumed that the desired location is a flyby offset towards the sun to maximize illumination and at a distance that results in the target filling one third of the closest approach image, with zero $LTOF$. A sensitivity matrix K is then calculated via finite differencing to relate a ΔV to the resulting effect in the B-plane. ΔV is then solved for as seen in equation 3.3. A more detailed breakdown of the mathematics just mentioned is given by Bhaskaran and Kennedy [1].

$$\Delta V = K^{-1} Z \tag{3.3}$$

3.6 **Terminal Guidance Sequencing**

The impactor maneuver sequencing in this thesis is derived from the Deep Impact mission [14], presented in Figure 3.3, which consisted of three burns, the first Impact-90 minutes. This allowed for enough observations to be collected to generate an accurate OD before the maneuver. The second burn is then at I-35 minutes, followed by the final burn at I-12.5 minutes. Delaying the time of this final burn can significantly improve impact success, however pushing the burn later can also leads to higher ΔVs as the spacecraft may have to deal with large handoff errors from the second burn. Between each burn, images are taken at regular intervals around 10 seconds apart to allow for processing time. The imaging sequence must also take into account any time required for the spacecraft to orient itself to perform the ΔV maneuver.

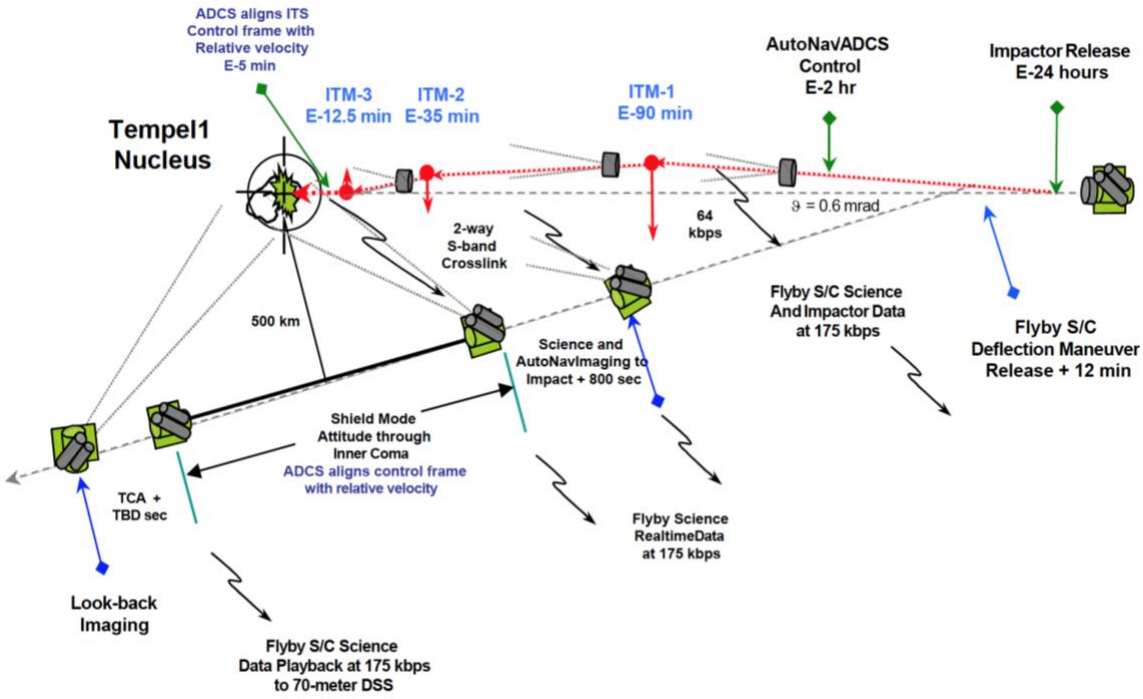

Figure 3.3: Deep Impact encounter with Tempel 1 [9].

The maneuver sequencing for the Deep Impact flyby spacecraft is much less complicated. As shown in Figure 2.4 the flyby spacecraft executed only one maneuver 12 minutes after detaching from the impactor, which occurred 24 hours before encounter. This is possible because delivery accuracy requirements to get good flyby images are far less intense than those for impacting and for Deep Impact those requirements could be satisfied with the knowledge levels 24 hours before encounter, which is typical with all small body encounters. For example, the most recent flyby was of Kuiper Belt object Arrokoth by New Horizons which executed its final maneuver nearly two months before encounter. However, determining delivery requirements for flybys is a complicated process that depends on the size of the object, the sciences goals, and instrumentation requirements. How far in advance of encounter those requirements can be met is then determined via a covariance analysis study that simulates a realistic radiometric tracking schedule and opnav campaign. While an important aspect of mission design, this analysis would be beyond the scope of this thesis. Instead I assumed that the initial state errors, described later in 5.2.1, at the beginning of terminal guidance are within the theoretical delivery requirement, and so no maneuvering of the flyby

spacecraft will be done during the terminal guidance phase. The objective is to purely update the knowledge to maximize close approach flyby images.

Chapter 4

ENCOUNTER SCENARIOS

To design and build a spacecraft before a unique target is identified means designing for all realistic object sizes, shapes, relative velocities, and phase angles that could present themselves. Again, the nature of ISOs' hyperbolic orbits presents a uniquely challenging environment never investigated from a navigational standpoint. The next sections establish first what the physical properties ISOs are assumed to have in this thesis, and then what their orbits imply for encounters.

4.1 **Size and Shape**

When considering the possible object sizes, the two references Oumuamua and 2I/Borisov provide a wide range, with Oumuamua estimated to be 250 meters long, and 2I/Borisov between 1.4 and 6.6 kilometers in diameter. With only two data points it is difficult to confidently constrain the potential size range of ISOs. However, as this range brackets the lower and upper bounds of known asteroids it is also used to bracket the range of ISOs simulated in this thesis. Other justifications for this assumption include the fact that as targets get into the multi-kilometer size range mission success becomes guaranteed and so the potential for larger ISOs is not a concern. Also, as ISO's get smaller than Oumuamua and their brightness drops it becomes much less likely that such objects will be detected with enough advanced warning for an intercept mission. Therefore, simulating sub-100-meter ISOs is not considered realistic. Bhaskaran and Kennedy's work also demonstrated almost 100% impactor success rates with a 300 m diameter object with a high phase angle of 140° and relative velocity of 12.5 km/s, and while ISOs are shown to have much higher relative velocities and phase angles than this, the results with a 300 m object suggest it is safe to use Oumuamua's size as the lower bound for simulated encounters. Ultimately three object average diameters were selected for investigation in this thesis: 200 m, 600 m, and 1,500 m.

Defining the realistic shapes to consider is made particularly difficult by the unprecedented 9:1 length to width ratio of Oumuamua and with 2I/Borisov's shape hidden by its cometary coma. While it is possible that the planetary mechanisms that eject these objects from their home systems consistently produce highly elongated objects there are currently no models that suggest this. And with there being only two data points, the best place to interpolate additional information from is the asteroid and comet population, for which the highest length to width ratio is around 4:1 with most objects being very well rounded. Therefore, for this thesis all objects are were assumed to have length to width ratios of 1.5:1, an assumption also made by Bhaskaran and Kennedy. The unique dimensions and encounter scenario of Oumuamua is also investigated separately from the general simulation space.

4.2 **Relative Velocity and Phase Angle**

Realistically constraining the encounter relative velocities and angles is a challenge as these objects can enter the solar system at potentially any angle, with a wide range of escape velocities, and distances from the sun. The trajectory to intercept one of these possible orbits is then dependent on how early detection is and where the Earth is relative to the object. Fully modeling all these possibilities and optimizing all the intercept trajectories could be a thesis in itself, and so instead this thesis establishes basic assumptions that realistically constrain spacecraft intercept trajectories and builds off the trajectory analysis performed by Seligman and Laughlin [24]. Based on their analysis of the optimal trajectory to intercept Oumuamua they establish the assumption that on average most intercepts will occur somewhere on the 1 AU sphere centered at the sun. This assumption is somewhat flawed in that it doesn't properly consider that launching on an inclined orbit to intercept an ISO above or below the ecliptic is often much more costly than intercepting on the ecliptic which is highlighted by the optimum intercept trajectories for both Oumuamua and 2I/Borisov which both have very low inclinations. Otherwise this assumption is well justified by several concepts outlined below:

1) With limited warning times there will be fundamentally very little time for a spacecraft to significantly deviate from Earth's orbit to intercept an ISO.
2) When dealing with objects in the same size category as Oumuamua, which if the population is comparable to asteroid size distributions are likely the vast majority of ISOs, only those with close approaches to the sun (~ 1 AU) will ever get bright enough to be consistently detected by LSST [7].
3) Intercept before these objects on their inbound trajectories require such early detections that it is likely infeasible. Thus intercept must occur after perihelion and during the object's path out of the 1 AU sphere.

These concepts are used in this thesis to justify defining the nominal orbit of the intercepting spacecraft as the Earth's orbit with an assumed intercept distance of 1 AU. While this will never be the case, it serves as a baseline from which the general geometry of encountering an ISO can be understood and then modified to account for the realistic variations of intercepting trajectories. When dealing with an object on an orbit like 2I/Borisov, this 1 AU assumption falls apart as the closest approach for 2I/Borisov is 1.9 AU. These trajectories will require especially early detection, but are not infeasible without large ISOs. The effects these trajectory scenarios have on the encounter space is therefore made sure to be encapsulated by variations applied to the nominal Earth orbit spacecraft trajectory. A breakdown of how these assumptions are applied in the encounter analysis is demonstrated in the remainder of this section.

There are three orbital parameters that define the ISO's trajectory as it leaves the 1 AU sphere; hyperbolic escape velocity (V_∞), radius of perihelion (r_p), and orbit inclination. Orbit inclination is defined as zero in this analysis as the encounter phase angle can be defined by the combination of two angles depicted in Figure 4.1; the first being the angle between the spacecraft to ISO vector and component of the ISO to Sun vector that lies on the plane formed by the spacecraft and ISO's trajectories. The second angle is then defined by the orientation of this plane with respect to the sun, referred to in this thesis as the encounter plane inclination. If this angle is increased at all, it

will reduce the encounter phase angle as the target is guaranteed to have illumination from either above or below. Therefore, by assuming the ISO has zero inclination the encounter plane inclination is also guaranteed to be zero, thus the potential phase angles are maximized which encapsulates the worst-case scenario encounter for any given escape velocity and radius of perihelion. Under this worst-case scenario framework, the range of realistic escape velocities addressed in this thesis is from 3 km/s to 70 km/s, while the radius of perihelion is constrained to be between 0.1 AU and 1 AU. It is also important to note that for each combination of escape velocity and radius of perihelion, the ISO can then also be either prograde or retrograde.

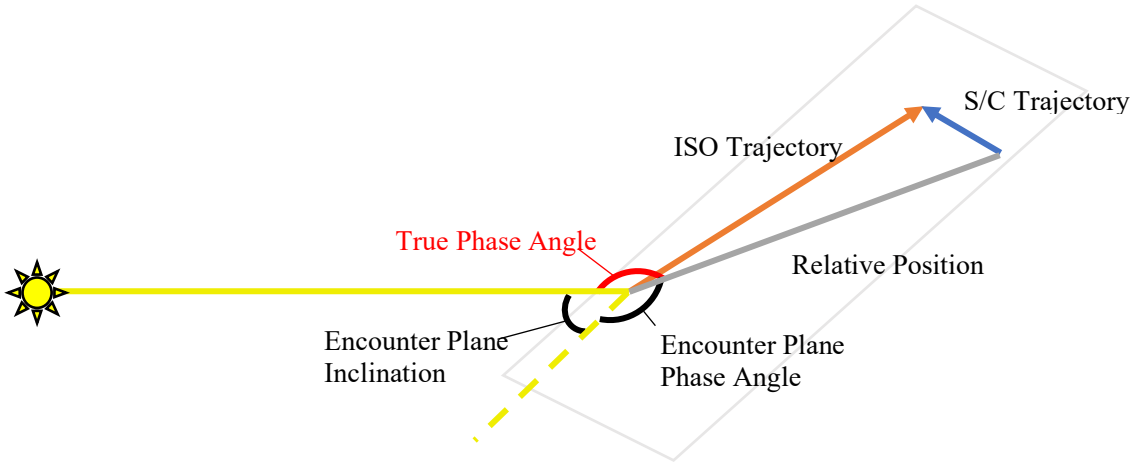

Figure 4.1: Encounter plane phase angle breakdown.

To translate these ranges of escape velocity and radius of perihelion to phase angle and relative velocity, first ISO flight path angle ($\emptyset$) and velocity (v) at 1 AU are calculated via basic orbital equations outlined in Appendix A. As the spacecraft is initially defined as always being on a circular intercept orbit at 1 AU, its flight path angle is zero and velocity is ~ 30 km/s. By approximating the final two hours of encounter as linear, the ISO and spacecraft flight path angles and velocities can then be used to define the encounter geometry. With the geometry defined, phase angle and relative velocity can be calculated as outlined in Appendix B. The realistic ranges of escape velocity and radius of perihelion can then be translated to the orange and blue nominal phase

angle and relative velocity regions plotted in Figure 4.2. The encounter space here is again a depiction of the worst-case scenarios with the spacecraft on the assumed nominal Earth orbit.

Real phase angles will likely always be less as inclination in the ISO or spacecraft orbits will translate to additional illumination. An inclined encounter plane can at most reduce the encounter phase angle to 90°, which is depicted and accounted for in the 'Inclined Encounter Plane' region in Figure 4.3. Also, if the spacecraft's intercept trajectory has a non-zero flight path angle, this too will affect the resulting relative velocity and phase angle. To expand the encounter space to include the effects of spacecraft trajectory variation, the median Earth departure velocity of 12 km/s as determined by Seligman and Laughlin is be applied as a vector to the Earth's velocity in all possible directions in the encounter plane. Applied perpendicularly this at most results in a flight path angle of 21.8° which serves to approximate the spacecraft's possible flight path angle deviation from zero. The resulting additional encounter scenario range is depicted as purple in Figure 4.3. These regions are then sampled as depicted to provide the particular encounter scenarios that are simulated.

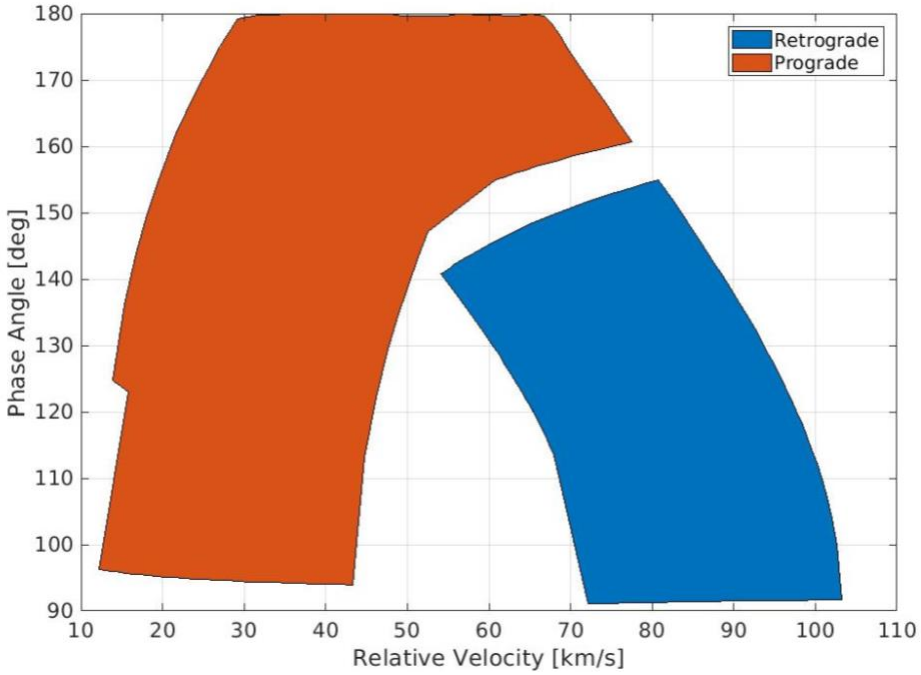

Figure 4.2: ISO hyperbolic escape velocity and radius perihelion mapped to worst case phase angle and relative velocity. (The gap is a result of the possible radius of perihelion being limited to 0.1 AU).

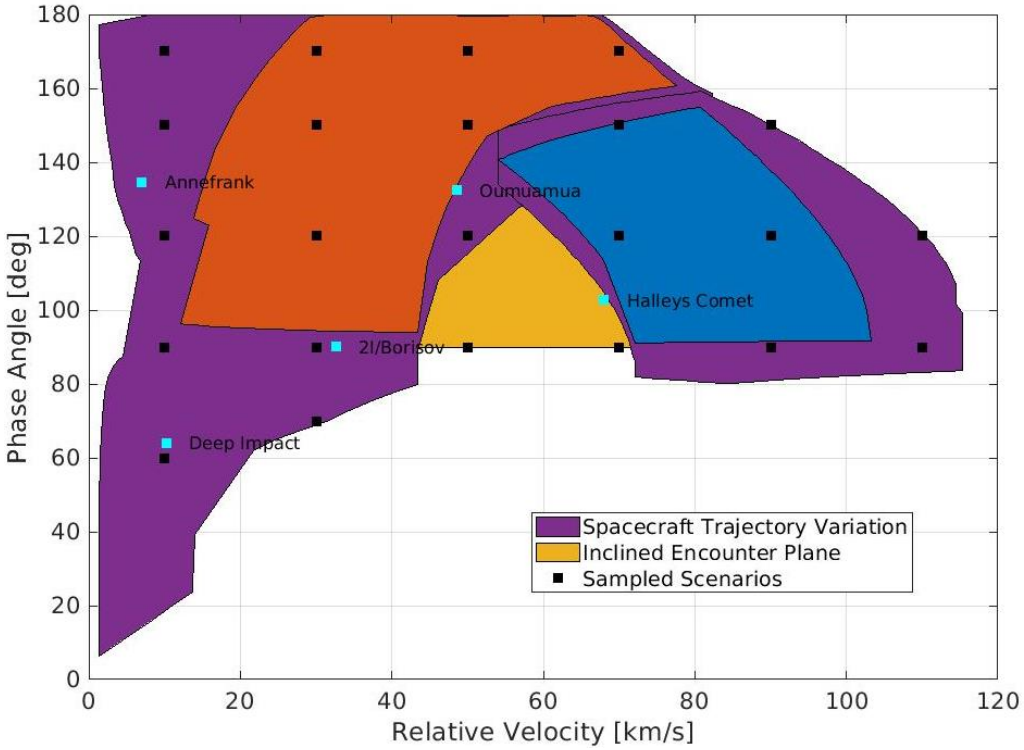

Figure 4.3: Possible encounter scenarios, factoring in variations in spacecraft trajectory and Sun location relative to encounter plane. Encounters scenarios for relevant real targets also plotted.

4.3 **ISO Brightness**

An important consideration for this thesis as demonstrated by Bhaskaran and Kennedy in their kinetic impactor study is the ability to do star relative navigation. While this thesis already attempts to take advantage of this form of attitude determination via 'flash-flash' photography, the potential high phase angles may translate to significantly dimmer targets such that stars can also be imaged in the background along with the target throughout the autonomous guidance phase. To better understand this possibility, Figure 4.4 was generated using the H-G magnitude system for asteroids [8] which defines the relationship between an asteroid's absolute magnitude, its reduced magnitude (H) which takes into account the asteroid-observer phase angle, and the apparent magnitude which then considers distance from the observer to the asteroid. The absolute magnitudes used to generate these results were taken from the JPL Small Body Database [33]. Information on the absolute magnitudes of all asteroids with sizes within 50m of the simulated ISO sizes was extracted and averaged to give an assumed absolute magnitude for each simulated ISO size. Then by applying the equations that define the H-G magnitude system, the apparent magnitude during approach is calculated. It is important to note that this method is meant to be used on asteroids with phase angles $< 120°$ as very little data exists on the brightness of asteroids at such high phase angles. The analysis of the phase curve of the Annefrank mission [6] gives one of the few examples of high phase asteroid brightness. The 150° phase and 170° phase lines are therefor likely not definitive in light of the lack of data on high phase-angle brightness, but as the goal of this analysis is to establish a baseline understanding of these encounters, the H-G magnitude system is probably sufficient.

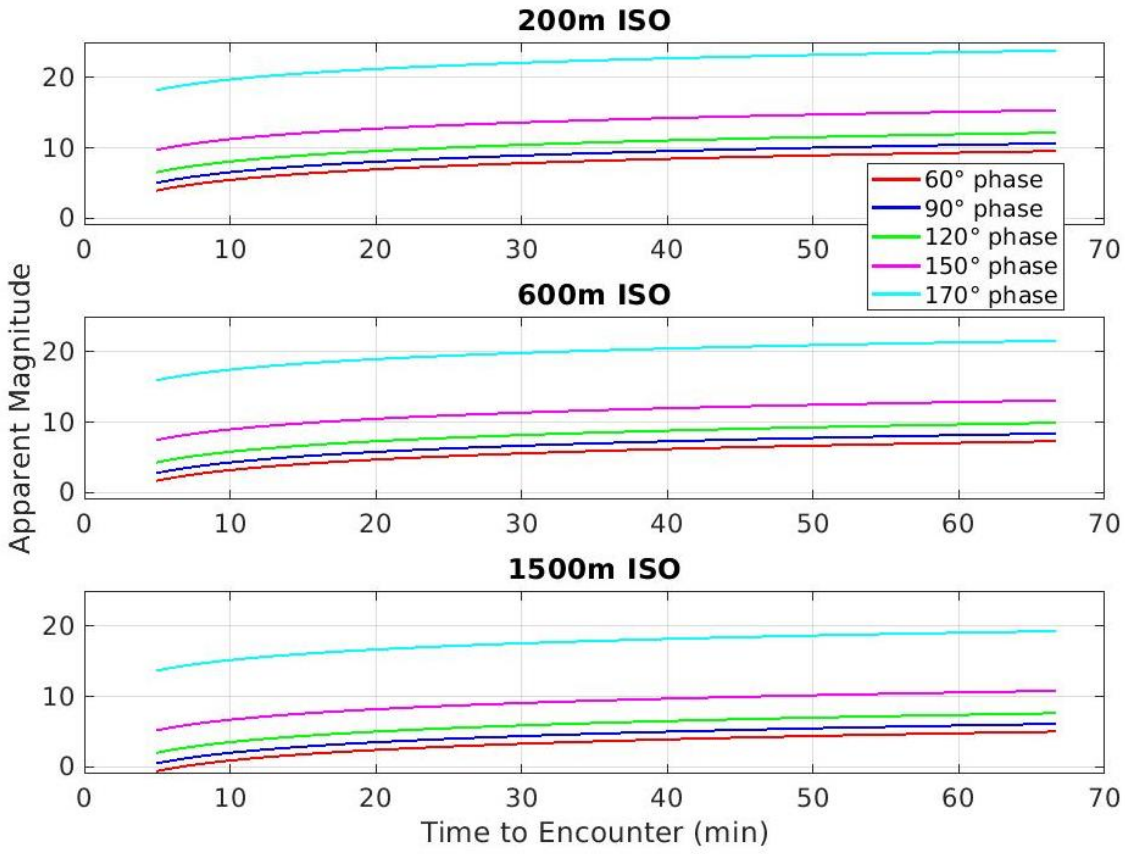

Figure 4.4: ISO apparent magnitude vs time to encounter, based on a 50 km/s relative velocity. Stops at 5 minutes from encounter as this is the final maneuver.

The apparent magnitudes shown in Figure 4.4 present both an additional challenge and a potential advantage to executing ISO encounters. The challenge comes primarily with the 170° phase angles where so little of the illuminated portion of the ISO is seen by the spacecraft that the apparent magnitude is almost 25 when the spacecraft is an hour away from encounter with a 200 m ISO. This is extremely dim and likely undetectable given current spacecraft capable camera technology. This is also amplified by the enormous relative velocity that results in the spacecraft simply being farther away from the ISO during approach. To relate these magnitudes to a real mission, the dimmest object ever navigated to was the Kuiper Belt object Arrokoth n 2019. At the beginning of the optical navigation campaign, more than three months before encounter, Arrokoth had an apparent magnitude of 19 [17]. It was only barely detectable even after combining 48 images of 30-second exposure, which translates to an effective 24-minute exposure time. Furthermore,

additional processing was necessary to subtract out background stars. Near the end of the approach, in the final optical navigation images Arrokoth had an apparent magnitude of 11 and was easily detectable with 0.5 s exposures.

Ultimately, as shown by this analysis, even larger ISOs could have similar apparent magnitudes and thus pose serious detection challenges when at high phase angles. The ability to observe these dim objects is defined by a complex relationship between optical instrument, detector sensitivity and noise characteristics, and tracking capabilities for longer exposures. It is also likely necessary to improve the understanding and brightness modeling of small bodies at high phase angles. Considering all this, while the design of an instrument to observe the potential dim magnitudes will be a very important aspect of the problem, such work would constitute another thesis topic entirely. As the focus of thesis is on the overall ability to navigate ISO encounters given relative velocity and phase angle, it is simply assumed that the signal strength of the ISO is observable throughout approach and so, while with current technology and techniques, it is likely impossible to detect a 200 m ISO at 170° and at 50 km/s this thesis will still analyze that encounter environment and all others regardless of apparent magnitude. As mentioned later in the conclusion aspect of this thesis a potential way to overcome these low visual magnitudes is the use of infrared imaging. Future work will likely have to emphasize the thermal modeling of ISOs and the potential detectability improvements of infrared at high phase angles.

To be more positive, Figure 4.4 also illustrates a potential advantage offered at higher phase angles and higher relative velocities. Usually the target is so bright during terminal guidance that it is impossible to image the background stars and the target at the same time. These background stars are ideally at least 9th apparent magnitude [19] and again referring to Figure 4.4, there are many scenarios where the target and background stars would be of similar brightness. For a 200 m ISO all phase angles could likely achieve this as at brightest the target is estimated to be around 5th magnitude at a 60° phase. Looking at the 600 m chart, while 170° phase clearly presents a detection

challenge, at 150° phase the ISO is right at the magnitude of ideal background stars and so both could confidently be imaged together. Down to 60° phase there may be potential for imaging the stars as well. Even 1500 m sized ISOs could present opportunities for background star imaging at higher phase angles. And while as ISOs get larger, they will inevitably reach magnitudes that wash out the stars, larger objects are fundamentally easier to navigate to in all other aspects. Overall this could be a powerful tool in enabling these missions as the errors from star relative navigation are an order of magnitude less than when using IMU propagation. However, a significant amount of work would need to be done before this can be implemented as there are numerous variables to consider. For a given encounter one must first know what the actual background stars will be and their apparent magnitudes. Those magnitudes, given the dynamic range of the imaging instrument, will give a range of ISO apparent magnitudes that can be imaged along with the stars. Then again, more work needs to be done improving our understanding of high phase angles and their effect on asteroid brightness as inaccuracies in this modeling could easily result in underexposed images and detection failure. This additional analysis is deemed outside the bounds of this thesis and is instead heavily recommended as a focus for future work. Since little can be said with confidence regarding when stars can and cannot be imaged, I take a conservative approach and assume the impactor only uses flash-flash imaging when attempting to derive attitude from the star field images.

Chapter 5

FLYBY AND IMPACTOR MONTE-CARLO ANALYSIS

5.1 **Overview**

In an initial attempt to characterize the challenges of a mission to an ISO, a broad Monte-Carlo analysis of a variety of the possible combinations of relative velocity, phase angle, object size, attitude determination method, and camera parameters, for both flyby and impactor spacecraft is performed. Each possible combination is then simulated 100 times, each time with a new sampling of the errors outlined in section 5.2. With each simulation the amount of 'successful encounters' is tracked. For the impactor spacecraft determining success/failure is simple as the impactor either hits the illuminated surface of the ISO or it does not. For the flyby spacecraft, success is more of a continuous regime defined by how many close approach images have the target in the field of view. This statistic is collected for each flyby simulation and is expressed as the percentage of images with the target in the field of view at a distance at which the target is at least 30 pixels across. This percentage is then averaged across the 100 simulations for each scenario.

5.2 **Inputs and Errors**

5.2.1 Initial Ephemeris and Errors

The initial ephemeris error refers to the error in the target relative state at the beginning of the terminal guidance phase. The target relative solution at that time is a combination of the ISO ephemeris from ground observations, the spacecraft ephemeris from radiometric tracking, and all optical navigation data collected during approach. As stated in section 2.2, the spacecraft's trajectory will typically have errors in the low tens of kilometers in position, with order of cm/s velocity error, while asteroids typically also have tens of kilometers position error and cm/s velocity error. However, the accuracy of an ISO's ephemeris cannot be assumed the same as typical

asteroids as an ISO's orbit inherently offers a much more limited time for observation. On the other hand, a mission like this would likely have unprecedented support from observatories in an effort to improve the target ephemeris as much as possible. A full orbit determination study on how these errors would map out to potential ISO orbits and sizes is also outside the bounds of this thesis, especially as these missions would likely rely on next generation observatories, and so I assume that for all simulated ISOs the initial ephemeris error is twice that assumed by Bhaskaran and Kennedy (Ref [1]), resulting in a 60 km 1σ position uncertainty and 10 cm/s 1σ velocity uncertainty. This uncertainty is sampled from a normal distribution and added to the nominal state of both the impactor spacecraft and flyby spacecraft.

For the impactor the nominal state is a trajectory that results in center of mass impact at the defined impact time. For the flyby spacecraft the nominal state is a trajectory offset such that it will produce a flyby distance that results in the illuminated side of the target ISO filling 1/3 of the imager's FOV. While the impactor spacecraft seeks to both refine the knowledge and perform maneuvers to eliminate the added error's effect on the B-plane, the flyby spacecraft only performs knowledge updates to enables accurate pointing during close approach. This does not change the fact that the initial added error to the nominal trajectory maps directly into the delivery location.

5.2.2 Maneuver Sequence and Execution Error

As stated earlier, the maneuver sequence implemented here is based on Deep Impact mission technique and follows a three-burn sequence. An initial burn is performed after an hour of observations are collected and one hour from impact, then a second burn is executed 30 minutes from impact, followed by the final burn at 5 minutes from impact. The timing of this sequence is not identical to Deep Impact as Deep Impact's target Tempel 1 was a multi-kilometer wide body. As some significantly smaller bodies are being targeted in this thesis, the sequence from Bhaskaran and Kennedy which implements somewhat later burns for additional accuracy is used instead.

When executing these burns in a real mission, there will always be a difference between a desired maneuver ΔV and the actual ΔV that results from firing thrusters. This difference can be the result of many factors including alignment errors, attitude errors, and timing error on startup and shutdown. The method of modeling these errors used by Bhaskaran and Kennedy and in this work is the Gates method. These error sources for ΔV are outlined in Table 5.1.

Table 5.1: Gates maneuver execution error model.

Parameter	Error Sampling (1σ)
Fixed Magnitude	4.3 mm/s
Proportional Magnitude	10%
Fixed Direction	4 mm/s
Proportional Direction	3.1%

5.2.3 Imaging Sequence and Attitude Determination Errors

There were three imaging sequences used in this broad initial analysis: one for the impactor when using the SSIMU for attitude determination, one for the impactor when using flash-flash attitude determination, and one for the flyby spacecraft while using the SSIMU. These sequences are outlined in Table 5.2. The sequence for the impactor SSIMU is again meant to mimic that of the Deep Impact impactor with images taken in increasing frequency leading up to impact. The impactor with flash-flash is derived from this sequence while taking into consideration that fewer images can be taken for target object observation since every other image is a longer exposure of the background stars as the target ISO brightness saturates the CCD. Again, as this has never been implemented before there is no precedent regarding the spacing between these images and so I assume a 50% increase in time between images after the first burn. The flyby spacecraft sequence is a simplified sequence of typical flyby imaging sequences. Images are initially taken at intervals similar to the impactor for state estimation, and then around the time the target is expected to extend to 30 pixels, rapid imaging takes place to collect as many images of the target as possible in these extremely fast encounters.

Table 5.2: Imaging sequences simulated during terminal guidance.

Spacecraft	Sequence: Time Between Images
Impactor - SSIRU	120s until T-60min : 30s until T-30min : 15s until T-5min
Impactor – Flash-Flash	120s until T-60min : 45s until T-30min : 22.5s until T-5min
Flyby Spacecraft	120s until T-60min : 30s until T-30min : 22.5s until 1.3x the time when target nominally has a width of 30 pixels : 5s until target stops filling 30 pixels on outbound trajectory

The two attitude determination methods considered in this thesis are again IMU propagation via the SSIRU and interpolation between target and background star imaging aka 'flash-flash'. The IMU errors begin accumulating at the start of each simulation and are characterized by the bias and angle random walk values listed in Table 5.3 for the SSIRU. The orbit determination filter is capable of estimating the bias while proper data weighting attempts to minimize the effects of the random walk. The errors associated with interpolating between background images on the other hand is not well characterized as this technique has never been implemented in a mission. In principle, there is an initial attitude error with the first background image, and another attitude error with the second. If the spacecraft has a constant attitude drift between these background star images, then the image taken of the target has an associated attitude error that is simply the average of the two background images' errors. However additional attitude error is introduced by vibrations within the spacecraft and any disturbances that might produce a non-linear path between images and so the attitude error assumed for this method is twice the assumed attitude error of the background images themselves, listed in Table 5.3.

In this thesis the flyby spacecraft is simulated using only the IMU for attitude determination as utilizing flash-flash imaging significantly reduces the number of well exposed images of the target and thus signifyingly reduces the science return. For the impactor spacecraft this is not as big a concern as the primary goal is to just achieve impact.

Table 5.3: Attitude determination errors.

Method	Associated Errors	
SSIRU Propagation	Rate Bias (1σ) (deg/hr)	Angle Random Walk (deg/$\sqrt{\text{hr}}$)
	0.0005	0.00005
Flash-Flash	Interpolation Error (1σ) $\frac{1}{5}$ IFOV	

5.2.4 Cameras

In attempting to determine what camera properties give high success rates this thesis first considers real flight heritage hardware used for previous flybys. These cameras, their description, and property of interest the IFOV are presented in Table 5.4.

Table 5.4: Existing cameras implemented in initial analysis.

Imager	Description	IFOV (μrad)
Medium Resolution Imager (MRI)	Used by the Deep Impact impactor spacecraft.	10.0
High Resolution Imager (HRI)	Used by the Deep Impact flyby spacecraft. Highest resolution imager ever flown.	2.0
Long Range Reconnaissance Imager (LORRI)	Used for the New Horizons flyby of Pluto and Arrokoth and to be used by the Double Asteroid Redirection Test's impactor spacecraft to Didymoon.	4.95

5.3 **Impactor Results**

First simulations were run utilizing the SSIRU for attitude determination, the results of which are outlined in Figure 5.1, where Green identifies ≥ 97% success rates, Yellow identifies ≥ 97% success rates with two impactors, Orange identifies ≥ 97% success rates with three impactors, Pink identifies the need for four or more impactors, and Red requires five or more.

SSIRU, 200m ISO

Relative Velocity	10 km/s			30 km/s			50 km/s			70 km/s			90 km/s			110 km/s		
Phase Angle	MRI	LORRI	HRI	MRI	LORRI	HRI	MRI	LORRI	HRI	MRI	LORRI	HRI	MRI	LORRI	HRI	MRI	LORRI	HRI
60°	88	86	89	24	22	22												
90°	66	66	69	22	19	19	4	8	8	2	2	3	1	1	2	1	1	2
120°	43	44	20	9	10	8	2	3	5	1	1	2	1	1	1	0	1	0
150°	12	18	7	3	4	1	1	0	2	0	0	1	0	0	0			
170°	0	0	2	1	0	0	0	0	0	0	0	0						

SSIRU, 600m ISO

Relative Velocity	10 km/s			30 km/s			50 km/s			70 km/s			90 km/s			110 km/s		
Phase Angle	MRI	LORRI	HRI	MRI	LORRI	HRI	MRI	LORRI	HRI	MRI	LORRI	HRI	MRI	LORRI	HRI	MRI	LORRI	HRI
60°	100	100	100	82	83	79												
90°	98	97	100	65	67	62	44	44	42	27	29	28	21	19	20	14	15	16
120°	85	86	86	46	47	45	29	30	27	12	11	14	9	7	9	3	5	6
150°	43	43	44	12	15	17	6	7	6	5	3	4	4	2	0			
170°	5	8	3	0	1	1	0	0	1	0	0	0						

SSIRU, 1500m ISO

Relative Velocity	10 km/s			30 km/s			50 km/s			70 km/s			90 km/s			110 km/s		
Phase Angle	MRI	LORRI	HRI	MRI	LORRI	HRI	MRI	LORRI	HRI	MRI	LORRI	HRI	MRI	LORRI	HRI	MRI	LORRI	HRI
60°	100	100	100	100	100	100												
90°	100	100	100	96	96	97	83	85	85	67	68	69	53	56	55	46	49	48
120°	99	99	100	80	80	83	63	61	63	47	51	50	37	41	42	30	32	32
150°	69	76	78	39	41	45	25	27	27	15	20	19	12	11	11			
170°	16	11	13	4	8	9	2	5	6	1	2	3						

Figure 5.1: Impact percentage success rates for 200 m, 600 m, and 1500 m ISOs utilizing various cameras and SSIRU for attitude determination. Green identifies >97% success rates, Yellow identifies >97% success rates with two impactors, Orange identifies > 97% success rates with three impactors, Pink identifies the need for four or more impactors for > 97% success rate, and Red requires five or more.

The challenge these encounters will present is immediately apparent. Attempting to impact the illuminated portion of a smaller 200 m ISO, with any imager is demonstrated to be infeasible using the same strategy as Deep Impact. At best, the HRI achieves an 89% illuminated impact success at 10 km/s and 60° phase. Using an IMU to propagate the attitude knowledge is only somewhat feasible in high probabilities in limited low relative velocity and low phase angles and with larger

ISOs. For a 600 m ISO high success rates are still only possible at 10 km/s, and only with a 1500 m ISO can high success rates be possible at 30 km/s. Ultimately, while the OD filter is able to estimate much of the attitude bias and drift, the random walk proves too significant almost immediately as the encounter scenarios get more challenging. This means that even with the HRI, the smallest IFOV ever flown on a flyby spacecraft, the attitude error will wash out its centerfinding accuracy, which is exemplified at the higher relative velocities and phase angles where the use of any of the three cameras results in effectively the same impact success. The gains with increased centerfinding accuracy from the camera simply plateau.

On the other hand, implementing a Flash-Flash attitude determination approach as shown in Figure 5.3 appears to be a very appealing alternative. First considering 200 m class ISOs, even with a lower resolution imager like MRI, reasonable success rates are achievable up to 90° phase and even at an extreme relative velocity of 90 km/s. When utilizing LORRI and even more so with HRI, high success rates can be achieved up to 120° phase and 110 km/s. For 600 m class ISOs the HRI extends the high success rates to 150° phase, while LORRI provides high success rates with two impactors. Going to 1500 m class ISOs, LORRI and HRI both provide 100% success rates no matter the relative velocity up to 150°, while even MRI provides high success with the use of two impactors up to 30 km/s.

However very notably, across all sizes and no matter the imager or attitude determination technique it is almost infeasible to impact the illuminated portion of an object at 170° phase. The challenge presented by such a high phase angle is highlighted in Figure 5.2, which shows how much of a spherical target is shadowed at various phases for a 600 m ISO and the distribution of impactor b-plane location (blue crosses). The reduction of area available to impact is one of the most limiting aspects of these high phase encounters. A phase angle reduces not only the total affective area but results in typically a very long thin illuminated region. Thus, in order to get high success rates an impactor's delivery distribution must be able to fit within the width of the region.

A rough estimate of this width for an assumed spherical ISO with radius *R* and phase angles greater than 90° is given in equation 4.1.

$$w = R - Rcos(180 - phase) \tag{4.1}$$

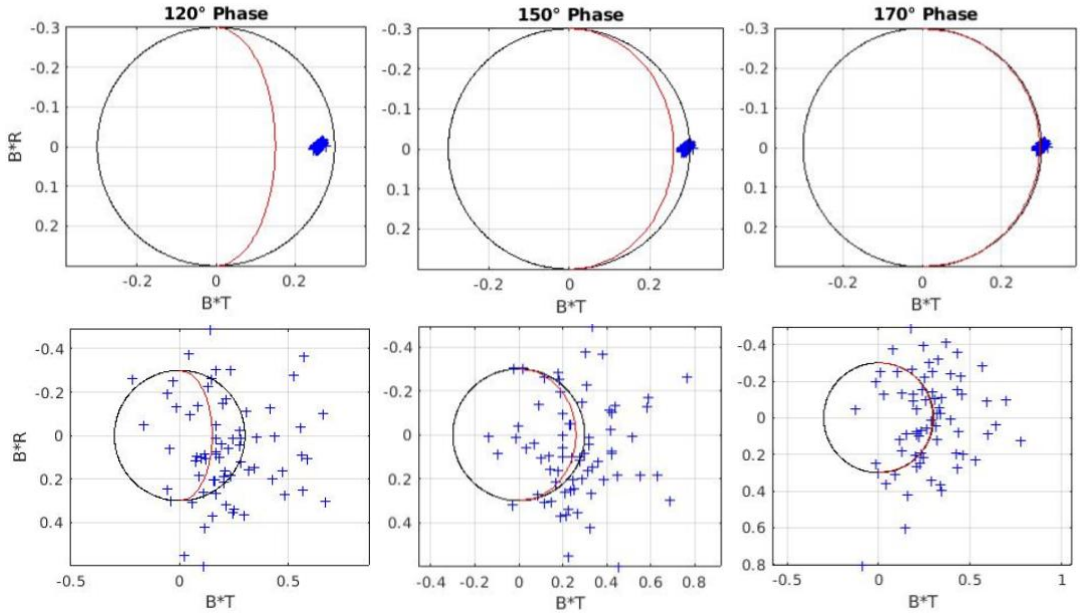

Figure 5.2: B-plane plots showing how terminator (red line) moves with increased phase angle. All plots show distributions at 50 km/s and using LORRI. Top row utilizes Flash-Flash and bottom the SSIRU.

The best performing spacecraft setup, the HRI with Flash-Flash imaging for attitude determination, produced a 3σ delivery accuracy of just under 20 meters at 70 km/s. Applying equation 4.1, we determine that in order to fit the 3σ distribution within the illuminated portion of a 170° phase spherical ISO, that ISO must at least be 2,360m in diameter. On the other hand, if the SSIRU is used to propagate attitude, even in combination with the HRI the best case 3σ delivery accuracy is 530m which requires a roughly 70km diameter ISO for high illuminated surface impact success rates. Illuminated impact is an enforced requirement as it guarantees the ejecta will also be illuminated. However as demonstrated by Deep Impact the ejecta can extend hundreds of meters above the target's surface. As a result, with a dark impact at least near the target's terminator line, the resulting ejecta would likely extend past the shadowed region and be partially illuminated for

flyby imaging. This potential loosening of the impactor delivery requirement could significantly improve success rates and is discussed as a topic of future work.

Flash-Flash, 200m ISO

Relative Velocity	10 km/s			30 km/s			50 km/s			70 km/s			90 km/s			110 km/s		
Phase Angle	MRI	LORRI	HRI	MRI	LORRI	HRI	MRI	LORRI	HRI	MRI	LORRI	HRI	MRI	LORRI	HRI	MRI	LORRI	HRI
60°	100	100	100	100	100	100												
90°	100	100	100	100	100	100	99	100	100	97	100	100	94	100	100	90	99	100
120°	100	100	100	94	99	100	86	97	100	81	91	100	75	89	99	68	86	99
150°	79	84	90	65	75	85	50	67	82	36	57	79	32	54	70			
170°	20	23	27	13	14	20	5	20	29	3	13	17						

Flash-Flash, 600m ISO

Relative Velocity	10 km/s			30 km/s			50 km/s			70 km/s			90 km/s			110 km/s		
Phase Angle	MRI	LORRI	HRI	MRI	LORRI	HRI	MRI	LORRI	HRI	MRI	LORRI	HRI	MRI	LORRI	HRI	MRI	LORRI	HRI
60°	100	100	100	100	100	100												
90°	100	100	100	100	100	100	100	100	100	100	100	100	100	100	100	100	100	100
120°	100	100	100	100	100	100	100	100	100	99	100	100	96	100	100	94	100	100
150°	96	100	100	91	99	100	80	93	99	74	89	98	65	84	97			
170°	34	35	37	31	34	47	16	32	46	9	31	39						

Flash-Flash, 1500m ISO

Relative Velocity	10 km/s			30 km/s			50 km/s			70 km/s			90 km/s			110 km/s		
Phase Angle	MRI	LORRI	HRI	MRI	LORRI	HRI	MRI	LORRI	HRI	MRI	LORRI	HRI	MRI	LORRI	HRI	MRI	LORRI	HRI
60°	100	100	100	100	100	100												
90°	100	100	100	100	100	100	100	100	100	100	100	100	100	100	100	100	100	100
120°	100	100	100	100	100	100	100	100	100	100	100	100	100	100	100	100	100	100
150°	98	99	100	99	99	100	98	100	100	94	100	100	88	100	100			
170°	33	73	78	55	63	69	43	57	67	27	50	65						

Figure 5.3: Impact percentage success rates for 200 m, 600 m, and 1500 m ISOs utilizing various cameras and Flash-Flash attitude determination. Green identifies >97% success rates, Yellow identifies >97% success rates with two impactors, Orange identifies > 97% success rates with three impactors, Pink identifies the need for four or more impactors for > 97% success rate, and Red requires five or more.

Another important consideration for the impactor encounter is the maneuvering ΔV. As the simulation simply calculates a maneuver and applies it, the resulting ΔVs must then be considered to determine if they are actually feasible. For each simulation the ΔVs of each maneuver are

collected, summed, and then averaged across the 100 Monte-Carlo runs. The results are presented in Table 5.5.

Table 5.5: Average total Delta-V for each combination of imager and attitude determination method versus the simulated relative velocities.

Imager	Attitude Determination Method	10 km/s	30 km/s	50 km/s	70 km/s	90 km/s	110 km/s
MRI	SSIRU	23.8	33.3	44.6	57.5	70.8	82.7
MRI	Flash-Flash	20.4	20.6	20.8	21.1	21.3	21.6
LORRI	SSIRU	23.5	32.5	43.2	54.7	67.1	79.8
LORRI	Flash-Flash	20.4	20.4	20.5	20.7	20.8	20.9
HRI	SSIRU	22.4	31.5	42.1	53.5	65.5	77.3
HRI	Flash-Flash	20.4	20.4	20.4	20.4	20.5	20.5

These results present high but not unreasonable ΔVs. For comparison, Deep Impact's total ΔV during the terminal guidance phase was 5.81 m/s. With the sampled state errors, each scenario on average has to remove 60 km of position error and 10 cm/s velocity error in each axis. When most of this error can be resolved before the first maneuver, we see that roughly 20 m/s of ΔV is required. This is highlighted by the fairly constant ΔV for all imagers when using flash-flash attitude determination. The overall observational accuracy when using this method enables the removal of almost all of the initial ephemeris error with the first burn even at the substantial distances this relates to at 110 km/s. The following burns then refine the targeting with slight adjustment maneuvers on the order of cm/s. However, when using the SSIRU there is a significant increase in ΔV as the relative velocities increase. The additional attitude error results in significant error in the state at the time of the first burn which then must be removed in the second and third burns. At the higher relative velocities, the final burn becomes much more costly as even at the time of the second burn the spacecraft can be over 100,000 km away. For example, at 90 km/s relative velocity, the observational accuracy at the time of the second burn is equivalent to the observational accuracy at 130 minutes from impact with 20 km/s relative velocity. Correcting this error with the last burn is

then expensive in ΔV. Optimizing the timing of the maneuvers for each encounter scenario can likely reduce these maneuvers significantly and will be a subject of future work. For now, the resulting ΔV demonstrate order of magnitude feasibility and the potential benefits of flash-flash attitude determination.

5.4 Flyby Results

As stated earlier in section 5.2.3, the flyby analysis focuses on using the SSIRU to propagate attitude and determines success based on the fraction of captured images that include the center of the ISO in the frame during the period when the ISO goes from being 30 pixels across on the inbound trajectory to the time it stops being 30 pixels across on the spacecraft's outbound trajectory. The spacecraft's ability to do this is defined by how accurately the spacecraft can determine its relative state to the target during the terminal phase so that during closest approach it knows where to point to get high-resolution images. However, with these high-speed flybys it is shown that knowledge errors can often cause the spacecraft to lose tracking of the ISO and miss portions of the close approach images. Specifically, the error of concern is the downtrack error, or how well the distance to the target is known. This is always the largest error as each image captures where the target is in the sky, but cannot directly measure how far away it is. As a result, the error ellipse of a target during approach will have the shape of a long pencil that is oriented towards the spacecraft. This error is primarily reduced during the closest approach period when the spacecraft starts to see the error ellipse from the side. The rapid elimination of this error is key to maintaining on target imaging during the closest approach. The challenge this presents is demonstrated in the rest of this section.

For each scenario, the percentages of images on target are collected and averaged across 100 encounter simulations and presented in Figure 5.4. Once again, a fairly grim picture is depicted by these success rates. In attempting to flyby a 200 m ISO only the HRI is on average capable of

getting more than 80% of the images of the target and only at the slowest relative velocity. That percentage drops to roughly 50% at the second lowest relative velocity and past that the percentages are unacceptably low, with the MRI even being incapable of getting any close approach images.

SSIRU, 200m ISO - (0.58 meters/pixel)

Relative Velocity	10 km/s			30 km/s			50 km/s			70 km/s			90 km/s			110 km/s		
Phase Angle	MRI	LORRI	HRI	MRI	LORRI	HRI	MRI	LORRI	HRI	MRI	LORRI	HRI	MRI	LORRI	HRI	MRI	LORRI	HRI
60°	64.9	78.2	83.8	15.2	32.8	49.4												
90°	64.5	77.9	83.6	14.9	32.3	49.5	0.0	16.8	24.6	0.0	0.0	14.3	0.0	0.0	8.9	0.0	0.0	6.1
120°	65.0	78.5	83.9	15.1	32.4	49.9	0.0	16.7	25.0	0.0	0.0	14.5	0.0	0.0	8.8	0.0	0.0	6.3
150°	65.0	78.9	84.8	15.6	33.0	48.5	0.0	17.0	25.7	0.0	0.0	14.8	0.0	0.0	8.9			
170°	64.8	77.9	83.6	16.3	33.8	48.0	0.0	17.8	27.9	0.0	0.0	16.2						

SSIRU, 600m ISO - (1.76 meters/pixel)

Relative Velocity	10 km/s			30 km/s			50 km/s			70 km/s			90 km/s			110 km/s		
Phase Angle	MRI	LORRI	HRI	MRI	LORRI	HRI	MRI	LORRI	HRI	MRI	LORRI	HRI	MRI	LORRI	HRI	MRI	LORRI	HRI
60°	92.8	98.2	100	62.9	75.2	89.8												
90°	92.4	97.8	100	62.9	75.0	88.7	38.6	55.0	73.6	24.2	38.7	65.5	14.3	26.8	49.4	9.7	18.3	39.1
120°	92.8	98.2	100	63.0	75.3	89.3	38.6	55.6	73.8	24.3	38.7	61.9	14.5	26.9	49.5	9.4	18.4	39.3
150°	93.2	98.4	100	64.0	76.9	89.9	38.3	56.5	75.6	24.5	39.0	62.3	14.0	27.1	49.0			
170°	91.8	96.4	100	63.9	77.4	89.7	37.9	54.9	76.3	23.9	37.7	60.2						

SSIRU, 1500m ISO - (4.4 meters/pixel)

Relative Velocity	10 km/s			30 km/s			50 km/s			70 km/s			90 km/s			110 km/s		
Phase Angle	MRI	LORRI	HRI	MRI	LORRI	HRI	MRI	LORRI	HRI	MRI	LORRI	HRI	MRI	LORRI	HRI	MRI	LORRI	HRI
60°	100	100	100	88.6	96.0	100												
90°	100	100	100	88.4	95.9	100	76.0	85.3	96.5	64.9	76.6	90.1	53.9	68.4	85.1	43.5	60.3	73.9
120°	100	100	100	88.9	96.3	100	76.8	85.7	97.2	64.8	76.9	90.7	54.3	68.9	85.5	43.5	60.6	74.2
150°	100	100	100	88.9	96.9	99.9	77.9	87.5	97.5	66.0	78.6	92.5	54.8	68.5	84.5			
170°	98.8	100	100	88.1	94.8	99.8	76.8	86.8	96.2	68.3	79.1	91.0						

Figure 5.4: Flyby close approach imaging percentage success rates for 200 m, 600 m, and 1500 m ISOs utilizing various cameras and SSIMU for attitude determination. Green identifies >80% of close approach images on target, Yellow identifies >60%, Orange identifies >40% and Red represents <40% close approach images on target.

The success of these flybys is most strongly limited by the speed at which they occur. The high speeds mean there is very little time spent close to the target to get enough images to pinpoint the

relative state to the levels required. This effect and the overall speed of these flybys is illustrated in Figure 5.5 and Table 5.6. which shows the how quickly ISOs change in pixel size during various encounters. It is also shown in the resulting success rates in Figure 5.4, which are clearly much more dependent on relative velocity than phase angle as the success rate variation with respect to phase is statistically insignificant.

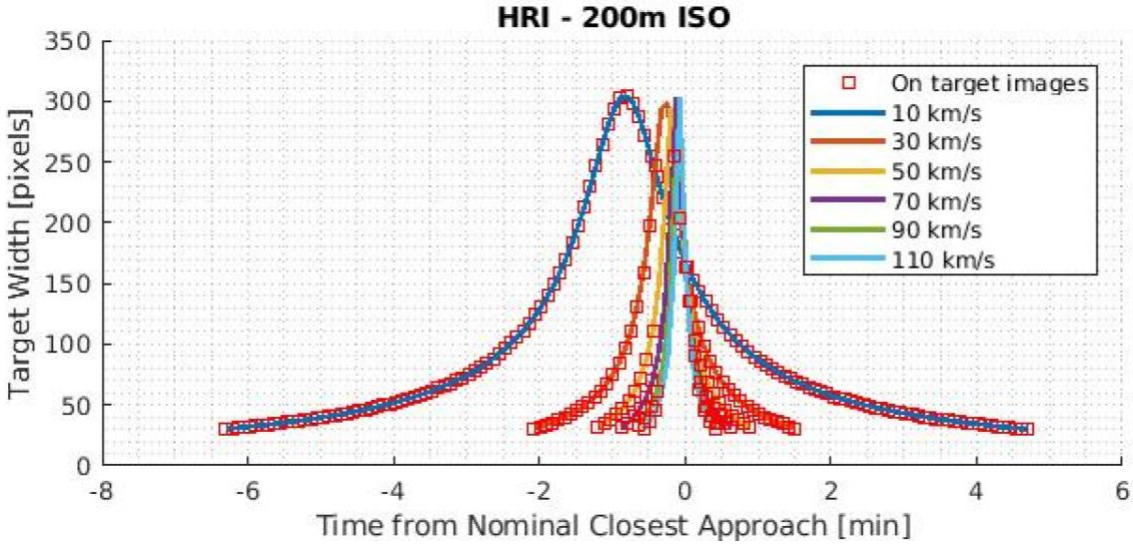

Figure 5.5: Encounter period of when ISO starts being 30 pixels across on inbound trajectory to when ISO stop being 30 pixels across on outbound trajectory.

Table 5.6: 200 m ISO encounter times for each imager vs simulated relative velocities.

Imager	10 km/s	30 km/s	50 km/s	70 km/s	90 km/s	110 km/s
MRI	2.22 min	0.75 min	0.45 min	0.32 min	0.25 min	0.21 min
LORRI	4.48 min	1.50 min	0.90 min	0.64 min	0.5 min	0.41 min
HRI	11.11 min	3.70 min	2.22 min	1.59 min	1.24 min	1.01 min

Even with the HRI, whose higher resolution allows for a more distant and thus longer flyby, the total time of encounter is only a couple of minutes at maximum. As shown, the encounters with speeds in excess of 30 km/s lose track of the ISO right as its resolution spikes and the downtrack error starts to be mapped into the image plane. While the flyby distance was set so the target filled 1/3 of the FOV, the size of is much less important compared to the desired spatial resolution of the

close approach images. For a flyby to result in a 200 m ISO filling 1/3 of the camera FOV, each pixel would have a spatial resolution of 0.58m, which implies that the area of the region within the entire FOV is then about 600 m x 600 m. Therefore, the relative state, including crucially the downtrack error (which is now completely mapped into the image plane), must be known to that precision. With a flyby at such high velocities, the spacecraft has very little time to observe the downtrack error and correct for it before it is mapped into the image field of view and the target is lost. Table 5.6 outlines how rapid these encounters are, giving the encounter times with a 200 m ISO for each imager at the simulated relative velocities. These short encounter times mean images must be taken rapidly to capture the downtrack error before it is too late. With the simulated 5 second intervals, the MRI only has time to take a couple of close approach images for most of the encounters. This presents a potential design constraint for fast imaging that may only be possible with CMOS detectors as opposed to more traditional CCDs. With larger simulated ISOs, the success rates do significantly improve. At 70 kms/s with a 600 m ISO and 1.76m/pixel, the HRI is able to get around 60% of the close approach images, which is a potentially acceptable rate. And once the resolution is above 4.4m/pixel, almost all the imagers start to enter the acceptable success rates range, while the HRI would perform well up to 90 km/s.

It is important to note that the standard deviations for these results, given in Appendix C, especially at the lower success rates can be very high. This stems from how the power of observation and difficulty to obtain observations increases during the encounter sequence. If the spacecraft's state error is small enough to get images on target past the initial 'ramp-up' mapping of the downtrack error period at the beginning of the curves in Figure 5.5, those images also increase in metric resolution at the same rate as the curves. Thus, if those images are on target, the knowledge gained enables the next image and so on. This leads to some 'all or nothing' results where if those images are collected on target, they can enable the collection of a high percentage of the total encounter images. On the other hand, if those initial images fail (are not on-target) then the remainder of the flyby will fail. This "all or nothing" behavior leads to bimodal Monte-Carlo

results with many instances of high success rates and many instances of very low success rates, resulting in high standard deviations in the averaged success rate. High average success rates and smaller standard deviations are produced when the knowledge is typically good enough to consistently capture those images after the initial ‘ramp up’ of metric resolution.

Chapter 6

INVESTIGATION OF ADDITIONAL FACTORS AND OUMUAMUA / 2I BORISOV

6.1 **Overview**

The broad initial analysis performed in the previous section established the fundamental baseline challenge these missions present and how the most important aspects of the spacecraft, the imager and the attitude determination method define success rates for simulated ISOs. This section investigates a few additional concepts, including the consideration of more phase angles to better understand how quickly impacting success rates drop from 140° to 170°, how an imagined "super high resolution" imager might improve success rates for a 200 m ISO flyby and impact, and the particular encounter scenarios of the only two known ISOs: Oumuamua and 2I/Borisov.

6.2 **Additional Phase Angles**

In Figure 5.3, the low success rates seen at 170° phase stand out as they drop significantly from those at 150° phase. Characterizing this drop is important as the high velocities of ISOs make phase angles between 150° and 170° are a very realistic possibility. To accomplish this the additional phase angles of 130°, 140°, 155°, 160°, and 165° are simulated at the same previous relative velocities while using flash-flash attitude determination with LORRI. The results are presented in Table 6.1. The success rates again demonstrate the challenge of achieving an illuminated impact with a small 200 ISO with a 130° phase effectively being the limit for high success rates. While for larger 1500 m class ISOs the higher phase angles between 150° and 170° are actually fairly reasonable as the drop in success rate appears to just start around 165°.

Table 6.1: Impact percentage success rates for 200 m, 600 m, and 1500 m ISOs at high phase angles between 130° and 165° utilizing LORRI and flash-flash attitude determination. Green identifies >97% success rates, Yellow identifies >97% success rates with two impactors, Orange identifies >97% success rates with three impactors, Pink identifies the need for four or more impactors for >97% success rate, and Red requires five or more.

		Relative Velocity				
	200 m ISO	10	30	50	70	90
Phase Angle	130°	99%	97%	92%	85%	81%
	140°	96%	92%	81%	77%	70%
	155°	78%	65%	42%	36%	
	160°	64%	44%	33%	23%	
	165°	44%	24%	20%	20%	

		Relative Velocity				
	600 m ISO	10	30	50	70	90
Phase Angle	130°	100%	100%	100%	99%	99%
	140°	100%	99%	99%	98%	94%
	155°	95%	95%	87%	77%	
	160°	90%	85%	76%	62%	
	165°	73%	70%	53%	53%	

		Relative Velocity				
	1500 m ISO	10	30	50	70	90
Phase Angle	130°	100%	100%	100%	100%	100%
	140°	100%	100%	100%	100%	100%
	155°	100%	99%	99%	97%	
	160°	100%	98%	96%	91%	
	165°	95%	91%	84%	81%	

6.3 Super Resolution Imager

The low encounter image percentages for the higher surface resolutions of 0.58 m/pixel and 1.76 m/pixel is a concern, as getting this close-up data will be the primary goal of the first ISO mission, regardless of whether an impactor is included. The results of the impactor simulations with the SSIRU depict a plateau in which additional accuracy from the imager has little effect past LORRI. But this plateau is not seen when using the SSIRU for a flyby and so the benefits of an

even higher resolution imager is assessed for a theoretical Super Resolution Imager (SRI) with a 0.5 μrad IFOV. Using the SRI, the encounters with 200

m, 600 m, and 1500 m ISOs were simulated with the resulting success rates presented in Table 6.2. Each scenario has an assumed 120° phase angle as the previous analysis showed that phase angle was not a significant factor.

Table 6.2: On target image percentages using the theoretical Super Resolution Imager.

		Relative Velocity					
		10 km/s	30 km/s	50 km/s	70 km/s	90 km/s	110 km/s
ISO Size	200 m, 0.58 m/pixel	90.9%	87.2%	70.4%	55.0%	43.5%	37.0%
	600 m, 1.76 m/pixel	100%	98.4%	93.6%	89.6%	83.1%	77.8%
	1500 m, 4.4 m/pixel	100%	100%	100%	100%	100%	100%

The gain in on-target image percentage is significant compared to the HRI. Where previously imaging at 0.58 m/pixel at 30 km/s was challenging, the added accuracy of the SRI and resulting longer encounter time is shown to be very powerful in enabling similar success rates out to 90 km/s. With this theoretical imager almost all 1.76 m/pixel cases are extremely successful and enable a much higher confidence in the ability to execute flybys with mid-sized ISOs. At the 4.4 m/pixel resolution for the 1500 m ISO, even at 110 km/s every image is on target.

6.4 Oumuamua and 2I/Borisov

While both Oumuamua and 2I/Borisov were detected after the time period during which launching on an intercept trajectory was feasible, it is worth considering those transfers and their associated encounter relative velocities and phase angles (Table 6.3) to ground the previous theoretical scenario simulations. Looking at Oumuamua first, its relative velocity and phase angle fits nicely within the broad simulation space as Oumuamua's trajectory and the spacecraft's

intercept trajectory follow the principles discussed in section 4.2. The intercept occurs very near to 1AU, the spacecraft has a small flight path angle, and the plane formed by Oumuamua's and the spacecraft's incoming trajectories is just slightly inclined.

Table 6.3: Encounter scenarios for Oumuamua and 2I/Borisov.

ISO	Ellipsoid Dimensions	Relative Velocity	Phase Angle
Oumuamua	520m x 58m x 58m	48.6 km/s	132.5°
2I/Borisov	3km x 3km x 3km	33.6 km/s	90.1°

However, Oumuamua does present a unique challenge that stems from its unprecedented roughly 9:1 elongation ratio. This elongation ratio does several things to make executing a mission difficult. First, while it may have a length or roughly 520m, the small width of roughly 58m is what drives the delivery accuracy requirement for impacting. On top of that Oumuamua has a rotational period of about 7.2 hours. As it rotates with its elongated body, the illuminated portion of its surface changes significantly, which will induce perceived motion in the center of brightness observables, which is then interpreted by the orbit determination filter as an incorrect relative motion.

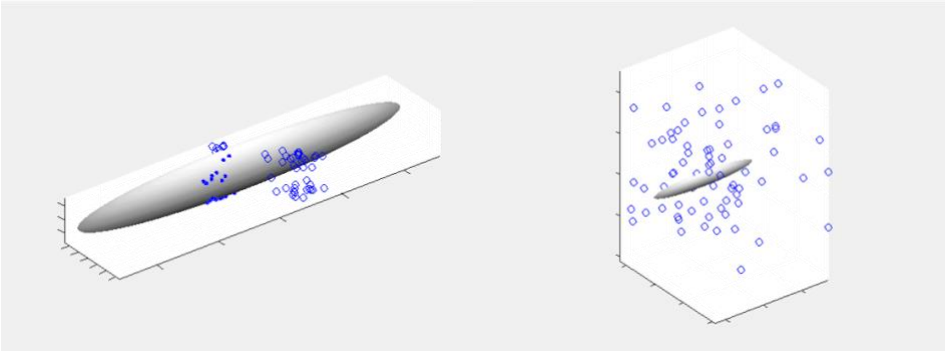

Figure 6.1: Delivery locations of impactor about Oumuamua for LORRI using flash-flash (left), and LORRI using the SSIRU (right).

The combination of these factors results in the poor impactor success rates in the table portion of Table 6.4 generated by 100 runs of the Monte-Carlo simulation. No combination of imager or attitude determination method provided any form of success. Only the theoretical Super Resolution

Imager produced success rates greater than 97% although for a mission with four impactors. In attempting to perform close approach imaging, the small width of Oumuamua is not a limiting factor and so moderate success rates are achievable. If highly elongated bodies are somehow are typical of ISOs through some yet unknown planetary formation process, then developing orbit determination filters designed to handle the perceived rotating brightness could help improve these rates.

Table 6.4: Success rates for the Oumuamua encounter for both impactor and flyby spacecraft.

Imager	Attitude Determination Method	Impact Success Rate	Imaging Success Rate
MRI	SSIRU	0%	39.2%
MRI	Flash-Flash	0%	
LORRI	SSIRU	0%	53.1%
LORRI	Flash-Flash	30%	
HRI	SSIRU	0%	76.8%
HRI	Flash-Flash	41%	
SRI	SSIRU	0%	81.3%
SRI	Flash-Flash	53%	

2I/Borisov presents a much easier encounter scenario compared to Oumuamua. Its orbit is highly inclined as it come down nearly perpendicular to the ecliptic, piercing the ecliptic plane at roughly 2AU. This is where a best transfer trajectory has the spacecraft intercepting 2I/Borisov. While it is much farther out than the assumed nominal 1AU intercept distance, the resulting encounter scenario is perfectly captured by the broad simulation space. Again, the spacecraft has a small flight path angle and a velocity well within the assumed +/- 12 km/s range from the Earth's orbital velocity while the resulting phase angle is described by the 'inclined encounter plane' region depicted in Figure 4.3. Both the relative velocity and phase angles are more favorable for success

compared to Oumuamua, and with the assumed size of 3 km, these factors result in a 100% success rates across all variations depicted in Table 6.5. Regardless of attitude determination method or imager, a kinetic impactor will collide with an illuminated portion of 2I/Borisov while the flyby spacecraft collects continuous, on-target close approach imaging. The distribution of impact

locations is depicted in Figure 6.2. The flash-flash method is extremely accurate with a very tight distribution of impact locations. Using the SSIRU and its associated errors, while an issue in previous encounter scenarios, does not prevent on-target illuminated impacts with such a large and well-lit body.

Table 6.5: Success rates for the 2I/Borisov encounter for both impactor and flyby spacecraft.

Imager	Attitude Determination Method	Impact Success Rate	Imaging Success Rate
MRI	SSIRU	100%	100%
MRI	Flash-Flash	100%	
LORRI	SSIRU	100%	100%
LORRI	Flash-Flash	100%	
HRI	SSIRU	100%	100%
HRI	Flash-Flash	100%	
SRI	SSIRU	100%	100%
SRI	Flash-Flash	100%	

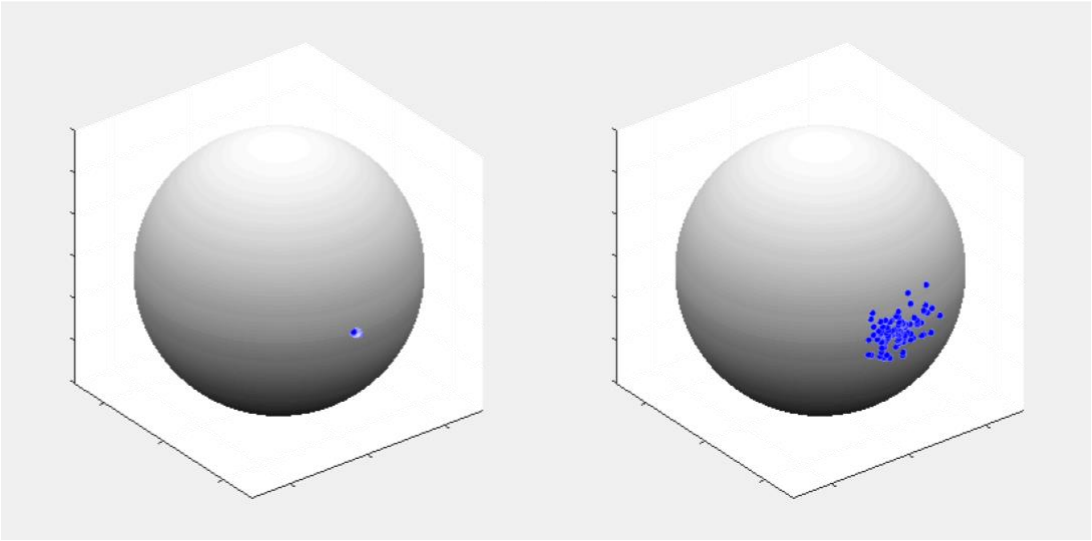

Figure 6.2: Delivery locations of impactor about the assumed 3km spherical ISO 2I/Borisov with the MRI using flash-flash (left), and MRI using the SSIRU (right).

Chapter 7

CONCLUSION

7.1 **Conclusions**

This thesis sought to establish a foundational understanding of the challenges that will be faced when attempting an impact/flyby encounter with a future ISO and how different equipment and techniques can enable this mission concept. As intercepting an ISO requires a 'launch on detection' paradigm, the spacecraft must be designed to perform in a wide range of potential encounter scenarios. The findings of this thesis first show that ISO hyperbolic orbits will likely result in these encounter scenarios being in the extremes of both relative velocity and phase angle. This presents a challenge to in deciding how much of the encounter space needs to be designed for. This is highlighted by the vastly different levels of difficulty presented by Oumuamua and 2I/Borisov. Designing for an ISO more similar to 2I/Borisov could result in an almost zero percent success rate if a smaller ISO on an orbit more like Oumuamua's shows up first. On the other hand, designing for Oumuamua and its reliance for success on significant improvements in an imager package would add significant cost to a mission that needs to be funded and built without a guaranteed target. The results of this thesis give an initial constraint on what fundamentally is and is not feasible and most importantly informs the direction of future work.

First, if a spacecraft is designed to use only the heritage processes implemented in Deep Impact then the region of potential ISO encounter scenarios in which the full impact and flyby can be executed will be severely limited. An impactor utilizing an IMU for attitude propagation cannot regularly achieve illuminated impact for any acceptable portion of the encounter space. The application of star-based attitude determination via flash-flash imaging was shown to be an extremely powerful alternative. While the number of observations of the target decreases, since the error is orders of magnitude lower than what is produced by IMU random walk, the result is huge

improvements to precise orbit determination. If applied to the impactor, success rates increase dramatically and give coverage of all the considered relative velocities and only fail at the most extreme phase angles. At these extreme phase angles around 160° to 170°, the size of sunlit surface becomes so small and thin that achieving illuminated impact requires unprecedented accuracies. I argued here that these results establish that flash-flash attitude determination is a requirement for the impactor.

For the flyby spacecraft the tradeoffs between using an IMU or attempting flash-flash is less definitive. While demonstrably feasible even with a lower resolution imager, without a powerful long-range imager spatial resolution will likely have to be reduced in order to get on-target images during closest approach. If there is a requirement to get the highest spatial resolution reasonably possible, there is also potential to apply flash-flash imaging initially during the terminal guidance phase and then switching to the SSIRU just before encounter. As demonstrated by the impactor analysis, flash-flash imaging can significantly increase knowledge accuracy. While this knowledge is still mostly in the cross-track direction, the tighter constraints on this error would allow for earlier identification of the downtrack error. There are some risks with attempting to use flash-flash for the flyby as an unexpected error in time-of-flight could result in the flyby spacecraft encountering the ISO sooner than expected and thus missing out on critical close approach images while longer exposures of the stars are being taken, especially as these flybys can start and end in less than a minute.

A summary recommendation informed by this work would be to design for the launch of multiple small and agile kinetic impactors, each equipped with a low-cost imager with resolutions comparable to the MRI. As also suggested by Seligman and Laughlin [24] this takes advantage of the fact that with such high relative velocities, the impactors can be small and still impart the necessary energy to generate similar ejecta to Deep Impact. By utilizing flash-flash attitude determination, each impactor will then have sufficient individual success rates that combined will cover all but the most extreme phase angles. The flyby spacecraft then is best equipped with at least

a LORRI class imager and SSIRU to take advantage of the benefits listed earlier that come with higher resolution imagers.

7.2 **Future Work**

With that recommendation there is also the caveat that a long list of things to still need to be investigated. There is a lot to add to these simulations to give the necessary confidence in the success rates for preliminary design, starting with the proper simulation of flash-flash imaging. While a conservative assumption is made regarding the errors when doing this, the actual generation of over-exposed images of the target and surrounding stars and autonomous processing of these images has not been investigated and needs to be done to give confidence in this thesis' simplified results. Overall additional complexity to the image simulation should be implemented to include complex shape models with varying albedos and shadowing effects. To give full validity to the simulation, non-linear orbital mechanics and perturbational effects should be implemented as well.

As mentioned in Section 3.8, further analysis also needs to be done on the brightness of these ISOs and how that pertains to detectability and the ability to avoid flash-flash imaging by simply imaging both the target and stars throughout the terminal guidance phase. The result of this analysis will likely eliminate the possibility of performing high phase angle flybys of smaller ISOs as they simply won't be detectable. It will also likely show that imaging the stars can be done for a large portion of encounter scenarios thus remove the need for the SSIRU for the flyby spacecraft and impactor. If the dimness of these targets is a limiting factor, then one might consider infrared imaging. This will also need to be heavily investigated and simulated to understand how ISOs' hyperbolic orbits affect object surface temperatures.

Another consideration for the high phase angle encounters is the illuminated impact requirement. Even if 170° phase objects can be reliably detected, the size of the sunlit surface becomes so small and thin that achieving consistent illuminated impact is impossible. As mentioned

earlier the ejecta will likely extend past the shadowed region even without illuminated impact. If the region of acceptable impact location can be extended outside the terminator line than success rates can improve dramatically and make impacting sub-kilometer ISOs at even the highest phase angles feasible. Thus, modeling dark impacts and understanding when the ejecta is sufficiently illuminated is a key topic of future research if an impactor is to be seriously pursued.

The constant improvement of our understanding of ISOs will also be critical to constraining this mission concept. As there are still only two known ISOs, the understanding of their population is expected to change significantly in the next decade as more discoveries are made. Some of the most important questions are where are they likely to come from? What are typical sizes and shapes? Will we be ready the next time one presents itself? A mission with such inherent risk will face serious challenges in acquiring funding from NASA and other space agencies. But while those political challenges are significant, the alternative of sending a spacecraft to another star system to collect data is infeasible with any current or foreseeable future technology. Thus, a flyby/impact of an ISO may be the only way to observe an object from outside of our solar system's bubble.

BIBLIOGRAPHY

[1] Bhaskaran, S., and Kennedy, B., "Closed loop terminal guidance navigation for a kinetic impactor spacecraft," Acta Astronautica, vol. 103, 2014, pp. 322–332.

[2] Bhaskaran, S., Mastrodemos, N., Riedel, J. E., & Synnott, S. P., "Optical Navigation for the STARDUST Wild 2 Encounter," International Symposium on Space Flight Dynamics, Oct. 2004.

[3] Bhaskaran, S., et al, "Navigation of the EPOXI spacecraft(?) to comet Hartley 2," Jet Propulsion Laboratory, Aug. 2011.

[4] Bhaskaran, S., "Autonomous Navigation for Deep Space Missions," SpaceOps 2012 Conference, 2012.

[5] Bergman, M., "New Horizons' Optical Navigation System". https://mattcbergman.com/2015/07/13/new-horizons-optical-navigation-system/ (2015)

[6] Carranza, E., Kennedy, B., Williams, K., "Orbit Determination of Stardust from the Annefrank Asteroid Fly-by through the Wild 2 Comet Encounter," AAS/AIAA Space Flight Mechanics Conference, Feb. 2004.

[7] Cook, N. V., Ragozzine, D., Granvik, M., and Stephens, D. C., "Realistic Detectability Of Close Interstellar Comets," The Astrophysical Journal, vol. 825, 2016, p. 51.

[8] Dymock, R., "The H and G Magnitude System for Asteroids," Journal of the British Astronomical Association, 2007, vol.117, no. 6, pp342-343.

[9] Frauenholz, R. B., Bhat, R. S., Chelsey, S. R., Mastrodemos, N., Owen, W. M., Ryne, M. S., "Deep Impact Navigation System Performance," Journal of Spacecraft and Rockets, Vol. 45, No. 1, 2008, pp. 39–56.

[10] Guzik, Piotr et al. "Initial Characterization of Interstellar Comet 2I/Borisov." Nature Astronomy (2019)

[11] Hein, A. M., Perakis, N., Eubanks, T. M., Hibberd, A., Crowl, A., Hayward, K., Kennedy, R. G., and Osborne, R., "Project Lyra: Sending a spacecraft to 1I/'Oumuamua (former A/2017 U1), the interstellar asteroid," Acta Astronautica, 2019.

[12] Ellis, J., McElrath T. P., "VEGA Pathfinder Navigation for Giotto Halley Encounter," The Telecommunications and Data Acquisition Report, 1986, pp 268-278

[13] Kantsiper, B., Cheng, A., and Reed, C., "The Double Asteroid Redirection test mission," 2016 IEEE Aerospace Conference, 2016.

[14] Kubitschek, D. G., "Impactor Spacecraft Encounter Sequence Design for the Deep Impact Mission," Jet Propulsion Laboratory.

[15] Mastrodemos, N., Kubitschek, D. G., and Synnott, S. P., "Autonomous Navigation for the Deep Impact Mission Encounter with Comet Tempel 1," Deep Impact Mission: Looking Beneath the Surface of a Cometary Nucleus, Dec. 2004, pp. 95–121.

[16] Moro-Martín, A., Turner, E. L., and Loeb, A., "Will The Large Synoptic Survey Telescope Detect Extra-Solar Planetesimals Entering The Solar System?," The Astrophysical Journal, vol. 704, 2009, pp. 733–742.

[17] Nelson, D. S., et al, "Optical Navigation Preparations for the New Horizons Kuiper-Belt Extended Mission," 2019.

[18] Newburn, R. L., Jr., et al., "Phase curve and albedo of asteroid 5535 Annefrank," J. Geophys. Res., 108(E11), 5117, doi:10.1029/2003JE002106, 2003.

[19] Owen, W. M., "Methods of Optical Navigation," AAS Spaceflight Mechanics Conference, Feb. 2011.

[20] Owen, W. M. Jr., Duxbury, T. C., Acton, C. H. Jr., Synnott, S. P., Riedel, J. E., Bhaskaran, S., "A Brief History of Optical Navigation at JPL," AAS paper 08–053, 31st Annual AAS Guidance and Control Conference, Breckenridge, CO, February 2008.

[21] Riedel et al., "Autonomous Optical Navigation (AutoNav) DS1 Technology Validation Report," Jet Propulsion Laboratory.

[22] Safronov, V. S., "The Motion, Evolution of Orbits, and Origin of Comets," SAO/NASA Astrophysics Data System, 1972.

[23] Schroeder, D. J., "Astronomical Optics, Second Edition," Academic Press, 1999.

[24] Seligman, D., and Laughlin, G., "The Feasibility and Benefits of In Situ Exploration of 'Oumuamua-like Objects," The Astronomical Journal, vol. 155, 2018, p. 217.

[25] Seligman, D., Laughlin, G., Batygin, K., "On the Anomalous Acceleration of 1I/2017 U1 'Oumuamua," ApJL, Mar. 2019.

[26] Trilling, D. E., Robinson, T., Roegge, A., Chandler, C. O., Smith, N., Loeffler, M., Trujillo, C., Navarro-Meza, S., and Glaspie, L. M., "Implications for Planetary System Formation from Interstellar Object 1I/2017 U1 ('Oumuamua)," The Astrophysical Journal, vol. 850, 2017.

[27] Wood, L.J, "The Evolution of Deep Space Navigation: 1962–1989," Advances in the Astronautical Sciences: Guid- ance and Control, 2008, Vol. 131, ed. M.E. Drews and R.D. Culp, Univelt, San Diego, 2008, pp. 285-308.

[28] Wood, L.J, "The Evolution of Deep Space Navigation: 1989–1999," Advances in the Astronautical Sciences: The F. Landis Markley Astronautics Symposium, Vol. 132, ed. J.L. Crassidis, et al., Univelt, San Diego, 2008, pp. 877-898.

[29] Wood, L.J, "The Evolution of Deep Space Navigation: 1999–2004," Advances in the Astronautical Sciences: Space- flight Mechanics 2014, Vol. 152, ed. R.S. Wilson, et al., Univelt, San Diego, 2014, pp. 827-847.

[30] Wood, L.J, "The Evolution of Deep Space Navigation: 2004–2006," Jet Propulsion Laboratory, 2017.

[31] Northrop Grumman. Scalable SIRU Family. https://www.northropgrumman.com/MediaResources/MediaKits/Satellite/Documents/SIRU_Family.pdf

[32] JPL Mission Design Tool. https://ssd.jpl.nasa.gov/?mdesign

[33] JPL Small Body Database. https://ssd.jpl.nasa.gov/sbdb.cgi

Appendix A

ISO FLIGHT PATH ANGLE AND VELOCITY CALCULATION

The following steps are used to calculate the flight path angle and velocity of an ISO at 1 AU given its escape velocity and radius of perihelion.

1. Calculate the orbit's semi-major axis. Here μ is the gravitational parameter of the Sun:

$$a = -\mu/v_\infty^2 \tag{A.1}$$

2. Calculate orbit eccentricity:

$$e = 1 - r_p/a \tag{A.2}$$

3. Calculated orbit true anomaly:

$$\theta = \cos^{-1}\left(\left(\frac{a(1-e^2)}{1AU} - 1\right)/e\right) \tag{A.3}$$

4. Flight Path Angle:

$$\emptyset_{ISO} = \tan^{-1}\left(\frac{e*\sin(\theta)}{1+e*\cos(\theta)}\right) \tag{A.4}$$

5. Velocity:

$$v_{ISO} = \sqrt{\mu\left(\frac{2}{1AU} - \frac{1}{a}\right)} \tag{A.5}$$

Appendix B

ENCOUNTER PHASE ANGLE AND RELTAIVE VELOCITY CALCULATION

The following steps were used to calculate the possible phase angles and relative velocities that would present themselves when attempting to intercept ISOs.

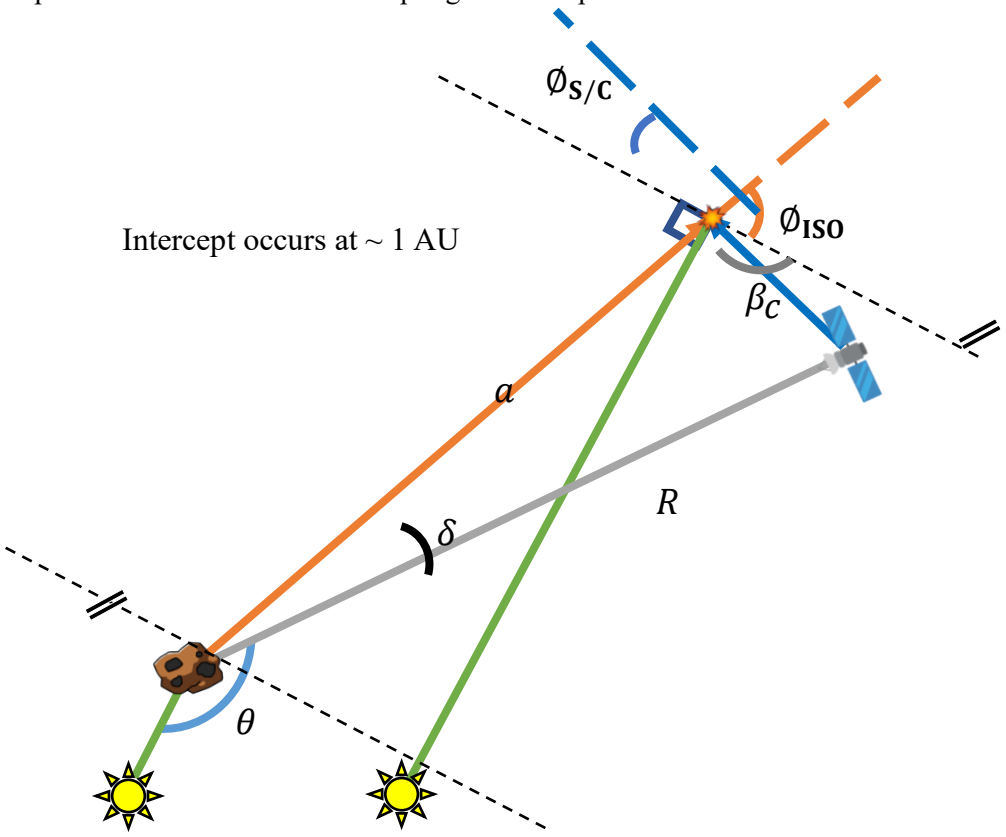

1. As the trajectories are assumed linear in the terminal guidance phase with t = 2 hours, the distance the ISO and S/C are from nominal encounter location are as such:

$$a = v_{ISO}\, t \quad \& \quad c = v_{SC}\, t \tag{B.1}$$

2. The angle β is then determined simply via the flight path angles of the ISO and spacecraft determined via steps in Appendix A:

$$\beta = 180 - \theta_{ISO} - \theta_{SC} \tag{B.2}$$

3. Looking at the triangle formed by $a, b, and\ R$ and using the law of cosines the distance from the ISO to the spacecraft is determined:

$$R = \sqrt{(v_{ISO}t)^2 + (v_{ISO}t)^2 - 2(v_{SC}t)(v_{ISO}t)\cos(\beta)} \quad \text{(B.3)}$$

4. The angle δ is then calculated via the law of sines:

$$\delta = \sin^{-1}\left(\frac{c\sin(\beta)}{R}\right) \quad \text{(B.4)}$$

5. Which gives the phase angle of the encounter:

$$\theta = 90 + \emptyset_{ISO} - \delta \quad \text{(B.5)}$$

6. And to complete the definition of the encounter, the relative velocity is derived as such:

$$V_{rel} = \frac{R}{t} \quad \text{(B.6)}$$

Appendix C

FLYBY SUCCESS RATE STANDARD DEVIATIONS

Table C.1: Flyby close approach imaging percentage success rate standard deviations for 200 m, 600 m, and 1500 m ISOs utilizing various cameras and SSIMU for attitude determination.

SSIRU, 200m ISO

Relative Velocity	10 km/s			30 km/s			50 km/s			70 km/s			90 km/s			110 km/s		
Phase Angle	MRI	LORRI	HRI	MRI	LORRI	HRI	MRI	LORRI	HRI	MRI	LORRI	HRI	MRI	LORRI	HRI	MRI	LORRI	HRI
60°	21.1	15.6	14.6	24.3	31.4	24.3												
90°	21.1	15.5	14.7	24.7	31.3	24.4	0.0	27.7	26.9	0.0	0.0	22.7	0.0	0.0	18.0	0.0	0.0	14.6
120°	20.6	15.6	14.9	25.3	31.2	24.8	0.0	27.5	27.1	0.0	0.0	23.0	0.0	0.0	18.1	0.0	0.0	14.6
150°	20.7	15.2	15.6	25.6	31.6	24.7	0.0	27.5	27.9	0.0	0.0	23.6	0.0	0.0	18.1			
170°	19.9	15.0	14.9	25.0	31.4	23.1	0.0	28.3	27.9	0.0	0.0	24.2						

SSIRU, 600m ISO

Relative Velocity	10 km/s			30 km/s			50 km/s			70 km/s			90 km/s			110 km/s		
Phase Angle	MRI	LORRI	HRI	MRI	LORRI	HRI	MRI	LORRI	HRI	MRI	LORRI	HRI	MRI	LORRI	HRI	MRI	LORRI	HRI
60°	7.4	3.1	0.0	19.3	14.2	8.3												
90°	7.6	3.4	0.0	19.6	14.1	8.3	27.3	22.9	14.3	26.3	26.9	19.6	22.6	28.0	23.8	20.3	25.9	25.6
120°	7.4	3.1	0.0	19.3	14.3	8.3	27.5	22.8	14.4	26.4	27.2	19.8	22.6	27.9	23.9	19.9	25.9	26.0
150°	6.8	2.8	0.5	19.7	14.2	8.1	27.4	22.9	14.4	26.1	27.1	19.5	23.7	28.0	23.8			
170°	7.5	4.2	0.3	18.2	12.8	8.6	26.7	20.1	13.0	26.1	26.9	16.8						

SSIRU, 1500m ISO

Relative Velocity	10 km/s			30 km/s			50 km/s			70 km/s			90 km/s			110 km/s		
Phase Angle	MRI	LORRI	HRI	MRI	LORRI	HRI	MRI	LORRI	HRI	MRI	LORRI	HRI	MRI	LORRI	HRI	MRI	LORRI	HRI
60°	0.0	0.0	0.0	8.7	5.0	0.0												
90°	0.0	0.0	0.0	8.7	5.1	0.0	13.1	9.7	4.4	18.3	13.0	7.7	22.9	16.2	9.9	26.9	19.0	14.3
120°	0.0	0.0	0.0	8.6	5.0	0.0	13.3	9.8	4.1	18.5	13.1	7.7	23.2	16.4	9.9	26.8	19.4	14.5
150°	0.3	0.0	0.0	8.3	4.3	0.8	13.3	9.4	4.0	18.1	12.8	7.1	23.2	16.2	9.5			
170°	2.0	0.0	0.0	9.1	5.5	0.9	12.3	9.8	5.1	15.0	11.7	8.0						